

PHYSICAL REVIEW D **79**, 113002 (2009)**Oscillations of very low energy atmospheric neutrinos**

Orlando L. G. Peres

*The Abdus Salam International Centre for Theoretical Physics, I-34100 Trieste, Italy  
Instituto de Física Gleb Wataghin - UNICAMP, 13083-970 Campinas SP, Brazil*

A. Yu. Smirnov

*The Abdus Salam International Centre for Theoretical Physics, I-34100 Trieste, Italy  
Institute for Nuclear Research of Russian Academy of Sciences, Moscow 117312, Russia*

(Received 14 April 2009; published 5 June 2009)

There are several new features in the production, oscillations, and detection of the atmospheric neutrinos of low energies  $E \lesssim 100$  MeV. The flavor ratio  $r$  of muon to electron neutrino fluxes is substantially smaller than 2 and decreases with energy, a significant part of events is due to the decay of invisible muons at rest, etc. Oscillations in a two-layer medium (atmosphere-Earth) should be taken into account. We derive analytical and semianalytical expressions for the oscillation probabilities of these “sub-sub-GeV” neutrinos. The energy spectra of the  $e$ -like events in water Cherenkov detectors are computed, and the dependence of the spectra on the 2-3 mixing angle  $\theta_{23}$ , the 1-3 mixing, and the  $CP$ -violation phase are studied. We find that variations of  $\theta_{23}$  in the presently allowed region change the number of  $e$ -like events by about 15%–20% as well as lead to distortion of the energy spectrum. The 1-3 mixing and  $CP$  violation can lead to  $\sim 10\%$  effects. Detailed study of the sub-sub-GeV neutrinos will be possible in future megaton-scale detectors.

DOI: [10.1103/PhysRevD.79.113002](https://doi.org/10.1103/PhysRevD.79.113002)

PACS numbers: 14.60.Lm, 14.60.Pq, 95.55.Vj

**I. INTRODUCTION**

Studies of the atmospheric neutrinos have been performed mainly at energies  $E \gtrsim (0.1\text{--}0.2)$  GeV. There are only a few results on neutrinos of lower energies  $E = (10\text{--}100)$  MeV. The fluxes of these neutrinos [1] have been computed recently by several different groups [2–6], and there are some differences in the results of computations.

The  $e$ -like events induced by the low energy atmospheric neutrinos have been detected by Super-Kamiokande [7–9]. About  $88 \pm 12$  events were produced by interactions of the atmospheric  $\nu_e$  and  $\bar{\nu}_e$  directly, and  $174 \pm 16$  events originated from decays of invisible muons. In turn, these muons are generated by the  $\nu_\mu$  flux with typical energies (150–250) MeV [8]. The liquid scintillation detector (LSD) put only an upper bound on the  $\bar{\nu}_e$  flux:  $F_{\bar{e}} < 5 \times 10^4 \text{ cm}^{-2} \text{ s}^{-1}$  [10] for the energy range  $12 < E < 26$  MeV.

As far as the oscillation effects are concerned, only the vacuum  $\nu_\mu - \nu_\tau$  oscillations have been taken into account in [7–9]. Also oscillations in a two-layer medium with constant densities relevant for low energy neutrinos have been considered [11].

The low energy atmospheric neutrinos were discussed as a background for detection of the relic supernova neutrinos [12] as well as future SN neutrino bursts [13].

In this paper, we perform a detailed study of the oscillations of the “sub-sub-GeV” atmospheric neutrinos in the complete  $3\nu$  context. The range below 100 MeV offers rather rich oscillation phenomenology. Although presently

the number of detected events is small, in the future, new large scale experiments can accumulate large enough statistics to extract new interesting information.

The paper is organized as follows. In Sec. II, we summarize properties of the neutrino fluxes at low energies, as well as parameters of the neutrino trajectories. We present relevant oscillation probabilities inside the Earth in Sec. III. The probabilities of  $3\nu$  oscillations in a two-layer medium (the atmosphere and the Earth) are derived in Sec. IV. In Sec. V, we consider averaging and integration of the probabilities over the angular variables. In Sec. VI, we present the  $\nu_e, \nu_\mu$  atmospheric neutrino fluxes at a detector. We then compute the numbers of  $e$ -like events as functions of energy, in water Cherenkov detectors induced by the direct  $\nu_e, \bar{\nu}_e$  interactions (Sec. VII) and via the invisible muon decays (Sec. VIII). We study dependence of observables on the oscillation parameters. In Sec. IX, we present the energy spectra of  $e$ -like events in the megaton-scale detectors. Discussion and conclusions follow in Sec. X. In Appendixes A, B, and C, we present analytic and semianalytic formulas for the oscillation probabilities.

**II. ATMOSPHERIC  $\nu$  FLUXES AND TRAJECTORIES**

Let us summarize the properties of the neutrino fluxes with  $E \lesssim 0.1$  GeV. In Fig. 1, we show the produced (without oscillations) fluxes of the electron neutrinos  $F_e^0$ , electron antineutrinos  $F_{\bar{e}}^0$ , muon neutrinos  $F_\mu^0$ , and muon antineutrinos  $F_{\bar{\mu}}^0$  as functions of the neutrino energy. The lines

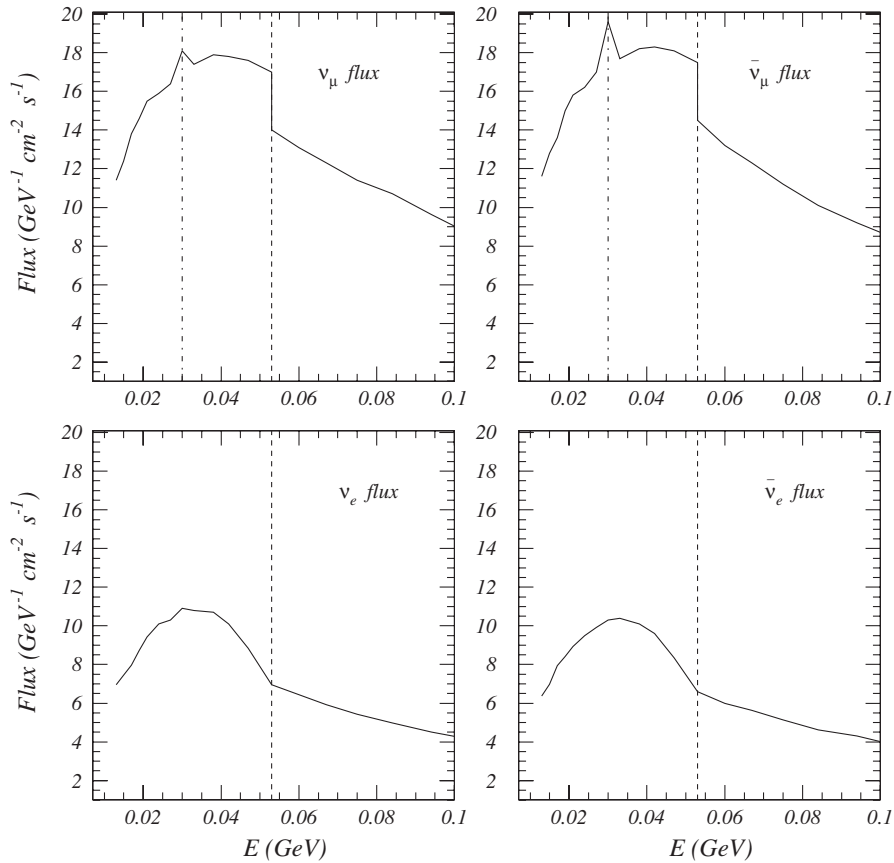


FIG. 1. The fluxes of  $\nu_\mu$ ,  $\bar{\nu}_\mu$ ,  $\nu_e$ , and  $\bar{\nu}_e$  neutrinos as functions of neutrino energy from [6]. The dashed vertical lines show the end point of the neutrino energy spectrum from the muon decay at rest  $E_\nu^\mu$  and the neutrino energy from the  $\pi$  decay at rest  $E_\pi^\pi$ .

have been drawn using the results of computations in Ref. [6]. The fluxes are averaged over the zenith and azimuthal angles. They depend on a period of solar activity which influences the fluxes of primary cosmic rays. Shown in the figure are the average values of neutrino fluxes during periods of the maximum and minimum of solar activity.

The low energy neutrino fluxes are formed mainly in the decays of pions and muons in flight and at rest. The  $K$ -meson decays contribute less than 0.05%. The key energy scales (indicated by the dashed lines in the figures) are the energy of muon neutrinos from the pion decay at rest,  $E_\nu^\pi \approx 30$  MeV, and the end point of the neutrino spectrum from the muon decay,  $E_\nu^\mu = 53$  MeV.

The properties of the spectra can be summarized as follows.

- (1) For  $E > E_\nu^\mu = 53$  MeV, the  $\nu_e$  and  $\bar{\nu}_e$  spectra are formed in muon decays in flight.
- (2) The bumps in  $\nu_e$  and  $\bar{\nu}_e$  spectra below  $E_\nu^\mu = 53$  MeV are due to the muon decay at rest. This contribution composes about 1/3 of the total flux at these energies.
- (3) The neutrino flux is slightly (5%–10%) larger than the antineutrino flux:  $F_\nu^0 > F_{\bar{\nu}}^0$ . The reason is that  $\nu_e$ 's originate from the chain of reactions  $\pi^+ \rightarrow \mu^+ \nu_\mu$ ,  $\mu^+ \rightarrow e^+ \nu_e \bar{\nu}_\mu$ , whereas  $\bar{\nu}_e$ 's are from the

conjugate reactions. Since the original cosmic rays are protons and nuclei, they overproduce  $\pi^+$  in comparison with  $\pi^-$ , and, consequently, the  $\pi^+$  chain is more abundant.

- (4) For  $E > 53$  MeV the muon (anti)neutrino spectra are formed by the pion and muon decays in flight. Since both the  $\pi^+$ - and  $\pi^-$ -decay chains produce an equal number of  $\nu_\mu$  and  $\bar{\nu}_\mu$ , the corresponding fluxes are approximately equal. The bump in the spectrum below  $E = 53$  MeV with a sharp edge at  $E = 53$  MeV is due to the muon decay at rest. The peak at  $E_\nu^\pi = 30$  MeV originates from the pion decay at rest. Below 30 MeV, the main contribution to the  $\nu_\mu$  flux is from the muon decay, and about 38% of the flux is generated by the pion decay in flight with neutrinos emitted in nonforward directions.
- (5) Below  $E_\nu^\mu$ , the  $\bar{\nu}_\mu$  flux is slightly larger than the  $\nu_\mu$  flux:  $F_{\bar{\nu}_\mu}^0 = 1.05 F_{\nu_\mu}^0$ . The difference originates from the muon decay at rest and has the same reason as the larger flux of  $\nu_e$ :  $\bar{\nu}_\mu$  comes from the chain  $\pi^+ \rightarrow \mu^+ \rightarrow \bar{\nu}_\mu$ .
- (6) According to [6], the  $\pi$ -decay peak for  $\bar{\nu}_\mu$  is larger than the  $\nu_\mu$  peak.

The flavor ratios

$$r(E, \Theta_\nu) \equiv \frac{F_\mu^0(E, \Theta_\nu)}{F_e^0(E, \Theta_\nu)}, \quad \bar{r}(E, \Theta_\nu) \equiv \frac{F_\mu^0(E, \Theta_\nu)}{F_{\bar{e}}^0(E, \Theta_\nu)} \quad (1)$$

play the key role in oscillations. Here  $\Theta_\nu$  is the zenith angle of neutrino trajectory. In what follows, we will discuss the ratios averaged over the zenith and azimuthal angles. As follows from Fig. 1, in the range  $E > E_\nu^\mu$  the ratios equal  $r \approx 2.0$  and  $\bar{r} \approx 2.2$ . Below  $E_\nu^\mu$ , the ratios decrease with energy. For instance, in maximum  $E \sim (35\text{--}40)$  MeV, one has  $r \approx 1.72$  and  $\bar{r} \approx 1.87$ ; for  $E = 21$  MeV, we obtain  $r \approx 1.65$  and  $\bar{r} \approx 1.77$ . This is an important difference from the case of higher energy atmospheric neutrinos, where  $r \sim 2$  and  $\bar{r} \sim 2.2$ .

In Fig. 2, we show the flavor ratio for the sum of neutrino and antineutrino fluxes:

$$\frac{F_\mu^\mu + F_{\bar{\mu}}^\mu}{F_e^0 + F_{\bar{e}}^0} \quad (2)$$

obtained from different computations. The ratio changes from 2 to almost 1.5, when the neutrino energy decreases from 100 to 10 MeV. The sharp jump of the ratio at 53 MeV is due to the muon decay spectrum which has a maximum at the end point.

There are differences between neutrino spectra presented by different groups. In Fig. 3, we compare the sum of  $\nu_e$  and  $\bar{\nu}_e$  fluxes from three available computations.

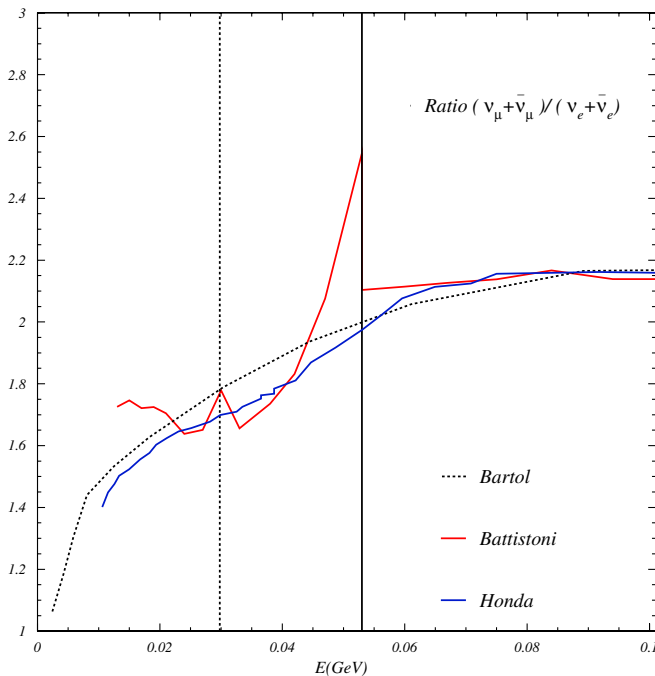


FIG. 2 (color online). The flavor ratio (2) obtained from results of computations of different groups: dashed line, Ref. [3]; red line, Ref. [6]; blue line, Ref. [5]. The vertical lines indicate the neutrino energy from the pion decay  $E_\nu^\pi$  (dashed) and the end point of the muon decay spectrum  $E_\nu^\mu$  (solid).

Notice that above 20–30 MeV the difference of spectra is about 10%–15%, and the shapes of spectra are rather similar. To have an idea about the solar activity effect, we show in Fig. 3 the fluxes in maximum and minimum of the activity computed by the Bartol group [3]. The difference is 15%–20%. In what follows, we will use the averaged over the solar cycle fluxes.

In contrast to high energies, for low energy neutrinos one needs to take into account the oscillations driven by the 1-2 mixing in the atmosphere. Indeed, the oscillation length is given by

$$l_\nu \equiv \frac{4\pi E}{\Delta m_{21}^2} = 10^3 \text{ km} \left( \frac{E}{30 \text{ MeV}} \right), \quad (3)$$

which is comparable to the length of trajectory in the horizontal direction.

The total length of neutrino trajectory from a production point to a detector  $L$  is given by

$$L^2 = 2R \left[ R \cos^2 \Theta_\nu + h - \cos \Theta_\nu \sqrt{R^2 \cos^2 \Theta_\nu + 2Rh + h^2} + \frac{h^2}{2R} \right], \quad (4)$$

where  $R$  is the radius of the Earth,  $h \sim 20$  km is the height in the atmosphere where neutrinos are produced, and  $\Theta_\nu$  is the zenith angle. We neglect here a depth of detector below the surface of the Earth.

Above the horizon,  $\cos \Theta_\nu > 0$ , trajectories are in the atmosphere only. In the horizontal direction,  $\cos \Theta_\nu = 0$ :

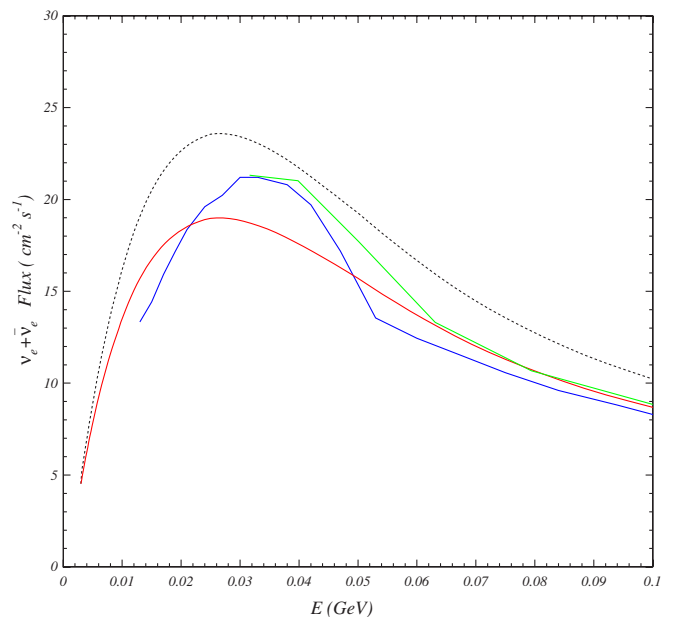


FIG. 3 (color online). The  $(\nu_e + \bar{\nu}_e)$  neutrino flux as a function of energy for the maximum (solid red line) and for the minimum (solid dashed line) of the solar activity from [3]. Shown also are the averaged over the solar activity cycle fluxes from [5]—Honda (green line)—and [6]—FLUKA (blue line).

$L = \sqrt{2Rh + h^2} \approx \sqrt{2Rh}$ . For trajectories below the horizon,  $\cos\Theta_\nu < 0$ , the length of trajectory inside the matter of the Earth equals

$$L_m = -2R \cos\Theta_\nu, \quad (5)$$

and for these trajectories the length in the atmosphere is

$$L_A(\cos\Theta_\nu) = L(\cos\Theta_\nu) - L_m(\cos\Theta_\nu) = L(-\cos\Theta_\nu). \quad (6)$$

For trajectories not very close to the horizon, we have  $L_A \approx h/\cos\Theta_\nu$ , which corresponds to the flat atmosphere and  $L \approx 2\sqrt{r(R\cos^2\Theta_\nu + h)}$ . The length of trajectory in matter and in the atmosphere become comparable:  $L_A = L_m \sim 500$  km at  $|\cos\Theta_\nu| \approx \sqrt{h/2R} = 0.04$ .

The half phases of oscillations in the atmosphere and the Earth equal

$$\phi = \pi \frac{L_A}{l_\nu}, \quad \phi^m = \pi \frac{L_m}{l_m}, \quad (7)$$

with  $l_\nu$  and  $l_m$  being the oscillation lengths in vacuum and in matter, correspondingly. Notice that at low energies the phase in the atmosphere cannot be neglected even for trajectories not very close to the horizon: For instance, for  $E = 30$  MeV and  $\cos\Theta_\nu = -0.3$ , we obtain  $\sin\phi = 0.2$ . For  $E = 60$  MeV, we have  $\sin\phi = 0.1$ . So, in general, at low energies the vacuum oscillation phase cannot be treated as a small parameter. The oscillations in the atmosphere can be neglected for the muon neutrinos producing the invisible muons.

### III. OSCILLATION EFFECTS INSIDE THE EARTH

Let us first consider the main features of oscillations at low energies inside the Earth. The resonance energy equals

$$\begin{aligned} E_R &= \frac{\Delta m_{21}^2 \cos 2\theta_{12}}{2V_e} \\ &= 96.4 \text{ MeV} \left( \frac{\Delta m_{21}^2}{7.3 \times 10^{-5} \text{ eV}^2} \right) \left( \frac{2.0 \text{ g/cm}^3}{Y_e \rho} \right) \\ &\quad \times \left( \frac{\cos 2\theta_{12}}{0.424} \right). \end{aligned} \quad (8)$$

So the energy interval  $E \lesssim 0.1$  GeV is at and below the 1-2 resonance. It is much below the 1-3 resonance:  $E/E_R^{(13)} \lesssim 0.015$ . As a consequence,

- (i) the matter effect on the 1-3 mixing is very small and can be neglected in the first approximation;
- (ii) the third eigenstate approximately coincides with the third mass eigenstate  $\nu_{3m} \approx \nu_3$ ;
- (iii) the state  $\nu_3$  decouples from dynamics and evolves independently. The two other states form a  $2\nu$ -mixing system, and so the problem is reduced to a  $2\nu$  problem;

- (iv) oscillations driven by the large mass split  $\Delta m_{31}^2$  are averaged out in probability due to integration over the angular variables and energy.

In what follows, we will quantify this picture and derive the relevant oscillation probabilities. The evolution of the neutrino flavor states  $\nu_f \equiv (\nu_e, \nu_\mu, \nu_\tau)^T$  is described by the equation

$$i \frac{d\nu_f}{dt} = \left( \frac{UM^2U^\dagger}{2E} + \hat{V} \right) \nu_f, \quad (9)$$

where the Pontecorvo-Maki-Nakagawa-Sakata mixing matrix defined through  $\nu_f = U\nu_{\text{mass}}$  can be parameterized as  $U = U_{23}\Gamma_\delta U_{13}U_{12}$ . Here  $\Gamma_\delta \equiv \text{diag}(1, 1, e^{i\delta})$ ,  $\hat{V} \equiv \text{diag}(V, 0, 0)$ ,  $V = \sqrt{2}G_F n_e$ , and  $U_{ij}$  is the rotation in the  $ij$  plane onto the angle  $\theta_{ij}$ .

Consider a new basis of states  $\nu' = (\nu'_e, \nu'_\mu, \nu'_3)^T$ , defined by

$$\nu_f = U'\nu', \quad (10)$$

where

$$U' \equiv U_{23}\Gamma_\delta U_{13}. \quad (11)$$

In this basis the Hamiltonian becomes

$$H' = \frac{1}{2E} U_{12} M^2 U_{12}^\dagger + U_{13}^\dagger \hat{V} U_{13}. \quad (12)$$

Taking into account that  $V s_{13} c_{13} \ll \Delta m_{31}^2/2E$ , we can perform the block diagonalization of  $H'$  in (12) which leads to

$$H' \approx \frac{1}{2E} U_{12} M^2 U_{12}^\dagger + \text{diag}(V c_{13}^2, 0, V s_{13}^2). \quad (13)$$

We use notations  $c_{13} \equiv \cos\theta_{13}$ ,  $c_{12} \equiv \cos\theta_{12}$ ,  $s_{12} \equiv \sin\theta_{12}$ , etc. The very small term  $-V c_{13}^2 s_{13}^2 (2VE/\Delta m_{31}^2)$  in the 11 element is neglected. [In this case the diagonalization is reduced to just omitting the off-diagonal elements in the second term of Eq. (12).] Essentially, this approximation corresponds to neglecting the matter effect on 1-3 mixing. The matter correction to the 1-3 mixing equals  $\theta_{13}(2VE/\Delta m_{31}^2)$  and, indeed, can be neglected [14]. According to (13), the state  $\nu_3$  decouples from the rest of the system and evolves independently. The two other states form the usual  $2\nu$  system with the Hamiltonian  $H_2 \equiv H_2(\Delta m_{21}^2, \theta_{12}, V c_{13}^2)$ . Therefore the  $S$  matrix (the matrix of amplitudes) in the basis  $\nu'$  has the following form:

$$S' \approx \begin{pmatrix} A'_{ee} & A'_{e\mu} & 0 \\ A'_{e\mu} & A'_{\mu\mu} & 0 \\ 0 & 0 & A_{33} \end{pmatrix}, \quad (14)$$

where

$$A_{33} = \exp(-i2\phi_3^m), \quad 2\phi_3^m = \frac{\Delta m_{31}^2 L_m}{2E} + V s_{13}^2 L_m, \quad (15)$$

and  $L_m$  is the total distance traveled by neutrinos in matter. The amplitude  $A'_{e\mu}$  describes the transition  $\nu'_{\mu} \rightarrow \nu'_e$ . The off-diagonal elements of  $S'$  equal each other:

$$A'_{\mu e} = A'_{e\mu}, \quad (16)$$

as a consequence of the  $T$  symmetry (the  $CP$  conservation in this basis and symmetry of the Earth matter profile). The amplitudes  $A'_{ee}$ ,  $A'_{e\mu}$ , and  $A'_{\mu\mu}$  are solutions of the evolution equation with the Hamiltonian  $H_2$ . As a consequence of unitarity,

$$A'_{\mu\mu} = A'^*_{ee}, \quad A'^*_{e\mu} = -A'_{e\mu}, \quad (17)$$

or  $\text{Re}A'_{e\mu} = 0$ ; that is, the transition amplitude is pure imaginary.

According to (10) the  $S$  matrix in the original flavor basis equals

$$S_f = U' S' U'^{\dagger}. \quad (18)$$

Therefore the  $\nu_{\alpha} \rightarrow \nu_{\beta}$  oscillation probability is given by

$$P(\nu_{\alpha} \rightarrow \nu_{\beta}) = |(U' S' U'^{\dagger})_{\beta\alpha}|^2. \quad (19)$$

Using  $U'$  defined in (11) and  $S'$  from (14) and averaging the oscillations related to the third mass eigenstate, we obtain explicitly

$$P(\nu_e \rightarrow \nu_e) = c_{13}^4 |A'_{ee}|^2 + s_{13}^4, \quad (20)$$

$$P(\nu_{\mu} \rightarrow \nu_e) = c_{13}^2 | -s_{13} s_{23} e^{-i\delta} A'_{ee} + c_{23} A'_{e\mu} |^2 + s_{13}^2 c_{13}^2 s_{23}^2, \quad (21)$$

and for the inverse channel:  $P(\nu_e \rightarrow \nu_{\mu}) = P(\nu_{\mu} \rightarrow \nu_e) \times (\delta \rightarrow -\delta)$ . Finally,

$$P(\nu_{\mu} \rightarrow \nu_{\mu}) = |c_{23}^2 A'_{\mu\mu} - s_{13} \cos\delta \sin 2\theta_{23} A'_{e\mu} + s_{13}^2 s_{23}^2 A'^*_{ee}|^2 + c_{13}^4 s_{23}^4. \quad (22)$$

Let us introduce three functions

$$\mathbf{D} \equiv \{P_2, R_2, I_2\} \quad (23)$$

(essentially the elements of the density matrix) as

$$P_2 \equiv |A'_{\mu e}|^2 = 1 - |A'_{ee}|^2, \quad R_2 \equiv \text{Re}(A'^*_{e\mu} A'_{ee}), \quad (24)$$

$$I_2 \equiv \text{Im}(A'^*_{e\mu} A'_{ee}).$$

These functions satisfy the relation

$$P_2^2 + R_2^2 + I_2^2 = P, \quad (25)$$

which follows from unitarity of the  $S$  matrix. The other properties of  $\mathbf{D}$  functions have been studied in [14].

According to (17) and (24)

$$\text{Re}(A'^*_{e\mu} A'_{\mu\mu}) = -R_2, \quad \text{Re}(A'^*_{\mu\mu} A'_{ee}) = \frac{1}{P_2} (I_2^2 - R_2^2). \quad (26)$$

By using these equalities and notations (24), the probabil-

ities (20)–(22) can be rewritten in terms of  $\mathbf{D}$  as

$$P(\nu_e \rightarrow \nu_e) = c_{13}^4 (1 - P_2) + s_{13}^4, \quad (27)$$

$$P(\nu_{\mu} \rightarrow \nu_e) = c_{13}^2 c_{23}^2 P_2 - s_{13} c_{13}^2 \sin 2\theta_{23} (\cos\delta R_2 + \sin\delta I_2) + s_{13}^2 c_{13}^2 s_{23}^2 (2 - P_2) \quad (28)$$

(which coincides up to the sign of  $\delta$  with the expression in Ref. [14]),<sup>1</sup>

$$P(\nu_{\mu} \rightarrow \nu_{\mu}) = 1 - 0.5 \sin^2 2\theta_{23} - c_{23}^4 P_2 + 2s_{13} \cos\delta \sin 2\theta_{23} (c_{23}^2 - s_{13}^2 s_{23}^2) R_2 + s_{13}^2 \sin^2 2\theta_{23} \left[ P_2 \cos^2 \delta + \frac{1}{2P_2} (I_2^2 - R_2^2) \right] - 2s_{13}^2 s_{23}^4 + s_{13}^4 s_{23}^4 (2 - P_2). \quad (29)$$

The first line in this equation is a sum of the averaged standard  $2\nu$ -oscillation probability  $\nu_{\mu} \rightarrow \nu_{\mu}$  driven by the 2-3 mixing, the contribution from the 1-2 oscillations for  $s_{13} = 0$ , and the first (linear in  $s_{13}$ ) correction due to the 1-3 mixing (the ‘‘induced’’ interference [14]). The probability (29) is an even function of  $\delta$ . Notice that in the second order the correlation of  $s_{13}$  and  $\delta$ :  $s_{13} \cos\delta$  is broken and these two parameters enter differently, which, in principle, opens a possibility to determine them independently.

For antineutrinos we have the same expressions for the probabilities with substitutions:  $\delta \rightarrow -\delta$ ,  $P_2 \rightarrow \bar{P}_2$ ,  $R_2 \rightarrow \bar{R}_2$ , and  $I_2 \rightarrow \bar{I}_2$ , where  $\bar{P}_2 \equiv P_2(V \rightarrow -V)$ , etc.

Some insight into properties of the probabilities and their dependence on the oscillation parameters can be obtained using expressions in the constant density case:

$$P_2^c = \sin^2 2\theta_{12}^m \sin^2 \phi^m, \quad R_2^c = -\frac{1}{2} \sin 4\theta_{12}^m \sin^2 \phi^m, \quad (30)$$

$$I_2^c = \frac{1}{2} \sin 2\theta_{12}^m \sin 2\phi^m,$$

where subscript ‘‘c’’ refers to the case of constant density and  $\phi^m$  is the half phase of neutrino oscillations in matter defined in (7). The probabilities for antineutrinos  $\bar{P}_2^c$ ,  $\bar{R}_2^c$ , and  $\bar{I}_2^c$  can be obtained from those in Eq. (30) by substituting  $\theta_m \rightarrow \bar{\theta}_m$  and  $\phi^m \rightarrow \bar{\phi}^m$ . The formulas for constant density (30) give a good qualitative and in many cases quantitative description of the results.

We compute the  $2\nu$  probabilities  $P_2$ ,  $R_2$ , and  $I_2$  and similar probabilities for antineutrinos numerically. A very precise semianalytical description of the probabilities can be obtained with the adiabatic Magnus expansion. In the first order of this expansion using the results of [15] [see Eqs. (78) and (76) in [15]], we obtain for the amplitudes in the  $\nu'$  basis

$$A'_{ee} = \cos I_{\theta} \cos \phi^{ad} + i(\cos I_{\theta} \sin \phi^{ad} \cos 2\theta_{12}^0 - \sin I_{\theta} \sin 2\theta_{12}^0), \quad (31)$$

<sup>1</sup>In our previous paper [14] we used a different definition of amplitudes,  $A_{\mu e}$  for the transition  $\nu_{\mu} \rightarrow \nu_e$ , instead of  $A_{e\mu}$ .

$$A'_{e\mu} = -i(\sin I_\theta \cos 2\theta_{12}^0 + \cos I_\theta \sin \phi^{ad} \sin 2\theta_{12}^0), \quad (32)$$

where  $\theta_{12}^0$  is the mixing angle in matter at the surface of the Earth,  $\theta_{12}^0 \equiv \theta^m(x_f)$ ,  $x_f$  is the surface coordinate, and

$$I_\theta = -2 \int_{\bar{x}}^{x_f} dx \left[ \frac{d\theta_{12}^m(x)}{dx} \right] \sin \phi^{ad}(x). \quad (33)$$

Here  $\bar{x}$  is the central point of the trajectory, and the expressions for probabilities are valid for a symmetric (with respect to  $\bar{x}$ ) density profile. The adiabatic half phase is given by

$$\begin{aligned} \phi^{ad}(x) &\equiv \frac{\Delta m_{21}^2}{4E} \int_{\bar{x}}^x dr \\ &\times \sqrt{\left( \cos 2\theta_{12} - \frac{2EV(r)c_{13}^2}{\Delta m_{21}^2} \right)^2 + \sin^2 2\theta_{12}}, \end{aligned} \quad (34)$$

and in Eqs. (31) and (32)  $\phi^{ad} \equiv \phi^{ad}(x_f)$ .

Using the amplitudes (31) and (32), we obtain the following expressions for  $P_2$ ,  $R_2$ , and  $I_2$ :

$$\begin{aligned} P_2 &= \cos^2 I_\theta \sin^2 2\theta_{12}^0 \sin^2 \phi^{ad} + \frac{1}{2} \sin 2I_\theta \sin 4\theta_{12}^0 \sin \phi^{ad} \\ &\quad + \sin^2 I_\theta \cos^2 2\theta_{12}^0, \end{aligned}$$

$$\begin{aligned} R_2 &= -\frac{1}{2} [\cos^2 I_\theta \sin 4\theta_{12}^0 \sin^2 \phi^{ad} + \sin 2I_\theta \cos 4\theta_{12}^0 \sin \phi^{ad} \\ &\quad - \sin^2 I_\theta \sin 4\theta_{12}^0], \end{aligned}$$

$$I_2 = \frac{1}{2} [\cos^2 I_\theta \sin 2\theta_{12}^0 \sin 2\phi^{ad} + \sin 2I_\theta \cos \phi^{ad} \cos 2\theta_{12}^0]. \quad (35)$$

These expressions are reduced to the expressions in (30) with substitutions  $\theta_{12}^m \rightarrow \theta_{12}^0$  and  $\phi^{ad} \rightarrow \phi^m$  if  $I_\theta = 0$  which would correspond to a perfect adiabaticity. From (35) we find formulas with the first nonadiabatic corrections:

$$\begin{aligned} P_2 &\approx \sin^2 2\theta_{12}^0 \sin^2 \phi^{ad} + I_\theta \sin 4\theta_{12}^0 \sin \phi^{ad}, \\ R_2 &\approx -\frac{1}{2} \sin 4\theta_{12}^0 \sin^2 \phi^{ad} - I_\theta \cos 4\theta_{12}^0 \sin \phi^{ad}, \\ I_2 &\approx \frac{1}{2} \sin 2\theta_{12}^0 \sin 2\phi^{ad} + I_\theta \cos 2\theta_{12}^0 \cos \phi^{ad}. \end{aligned} \quad (36)$$

For completeness in Appendix A we present also results in the second order of the Magnus expansion which provides better than 1% accuracy for all neutrino energies.

The results of this section can be used immediately for high energy neutrinos  $E > 150$  MeV and for trajectories far from the horizon, when oscillations in the atmosphere can be neglected.

#### IV. OSCILLATION EFFECTS IN THE ATMOSPHERE AND INSIDE THE EARTH

Above the horizon, the oscillations occur in vacuum (we neglect density of the atmosphere). The evolution of neutrinos can be considered again in the  $\nu'$  basis, since the connecting matrix  $U'$  depends on the vacuum mixing angles only.

Again, in the  $\nu'$  basis the third mass state decouples, and for two other states the  $2 \times 2$  block of the  $S$  matrix is given by

$$S_A^{(2)} \approx \begin{pmatrix} c_\phi + i \cos 2\theta_{12} s_\phi & -i \sin 2\theta_{12} s_\phi \\ -i \sin 2\theta_{12} s_\phi & c_\phi - i \cos 2\theta_{12} s_\phi \end{pmatrix}. \quad (37)$$

Here  $s_\phi \equiv \sin \phi$ ,  $c_\phi \equiv \cos \phi$ , and the half phase  $\phi$  is defined in (7). The oscillation probabilities in the flavor basis are given by the expressions (27)–(29) with  $P_2 = \sin^2 2\theta_{12} \sin^2 \phi$ ,  $R_2 = -\frac{1}{2} \sin 4\theta_{12} \sin^2 \phi$ , and  $I_2 = \frac{1}{2} \times \sin 2\theta_{12} \sin 2\phi$ .

For trajectories below the horizon, one needs to take into account oscillations in two layers: the atmosphere and the Earth. For these trajectories the total  $S$  matrix in the  $\nu'$  basis equals

$$S_{\text{tot}} = S' \cdot S_A \approx \begin{pmatrix} \tilde{A}_{ee} & \tilde{A}_{e\mu} & 0 \\ \tilde{A}_{\mu e} & \tilde{A}_{\mu\mu} & 0 \\ 0 & 0 & \tilde{A}_{33} \end{pmatrix}, \quad (38)$$

where  $S'$  is given in (14) and  $S_A$  describes evolution in the atmosphere.

Using the expressions for the amplitudes (B1) from Appendix B and properties of the amplitudes for a single symmetric layer (17), we obtain the relations

$$\tilde{A}_{\mu\mu} = \tilde{A}_{ee}^*, \quad \tilde{A}_{\mu e} = -\tilde{A}_{e\mu}^*. \quad (39)$$

The flavor oscillation probabilities can be computed according to  $P(\nu_\alpha \rightarrow \nu_\beta) = |(U' S_{\text{tot}} U'^\dagger)_{\beta\alpha}|^2$ . As a result, we obtain formulas similar to those in (27)–(29) for a single layer with, essentially, the substitution  $A'_{\alpha\beta} \rightarrow \tilde{A}_{\alpha\beta}$ :

$$P(\nu_e \rightarrow \nu_e) = c_{13}^4 |\tilde{A}_{ee}|^2 + s_{13}^4, \quad (40)$$

$$\begin{aligned} P(\nu_\mu \rightarrow \nu_e) &= c_{13}^2 | -s_{13} s_{23} e^{-i\delta} \tilde{A}_{ee} + c_{23} \tilde{A}_{e\mu} |^2 \\ &\quad + s_{13}^2 c_{13}^2 s_{23}^2, \end{aligned} \quad (41)$$

$$\begin{aligned} P(\nu_e \rightarrow \nu_\mu) &= c_{13}^2 | -s_{13} s_{23} e^{i\delta} \tilde{A}_{ee} + c_{23} \tilde{A}_{\mu e} |^2 \\ &\quad + s_{13}^2 c_{13}^2 s_{23}^2, \end{aligned} \quad (42)$$

$$\begin{aligned} P(\nu_\mu \rightarrow \nu_\mu) &= |c_{23}^2 \tilde{A}_{\mu\mu} - i s_{13} \sin 2\theta_{23} \text{Im}(e^{i\delta} \tilde{A}_{e\mu}) \\ &\quad + s_{13}^2 s_{23}^2 \tilde{A}_{ee}|^2 + c_{13}^4 s_{23}^4. \end{aligned} \quad (43)$$

In the last equation, we used the properties (39).

Since the two-layer density profile is not symmetric, we have inequality  $\tilde{A}_{\mu e} \neq \tilde{A}_{e\mu}$ , and, furthermore, these amplitudes are not pure imaginary. Consequently, the probabilities (27)–(43) are expressed now in terms of 5 different functions

$$\tilde{\mathbf{D}} \equiv \{\tilde{P}, R_{e\mu}, R_{\mu e}, I_{e\mu}, I_{\mu e}\}, \quad (44)$$

and not three  $\mathbf{D}$ , as in the case of symmetric profile. We introduce them as

$$\begin{aligned}\tilde{P} &\equiv |\tilde{A}_{\mu e}|^2 = |\tilde{A}_{e\mu}|^2, & R_{e\mu} &\equiv \text{Re}(\tilde{A}_{e\mu}^* \tilde{A}_{ee}), \\ I_{e\mu} &\equiv \text{Im}(\tilde{A}_{e\mu}^* \tilde{A}_{ee}), & R_{\mu e} &\equiv \text{Re}(\tilde{A}_{\mu e}^* \tilde{A}_{ee}), \\ I_{\mu e} &\equiv \text{Im}(\tilde{A}_{\mu e}^* \tilde{A}_{ee}).\end{aligned}\quad (45)$$

From unitarity of the  $S$  matrix we have  $|\tilde{A}_{\mu\mu}|^2 = |\tilde{A}_{ee}|^2 = 1 - \tilde{P}$  and  $\tilde{A}_{ee} \tilde{A}_{\mu e}^* = -\tilde{A}_{e\mu} \tilde{A}_{\mu\mu}^*$ . In turn,  $\tilde{P}$ ,  $R_{e\mu}$ ,  $I_{e\mu}$ ,  $R_{\mu e}$ , and  $I_{\mu e}$  are the functions of  $P_2$ ,  $R_2$ , and  $I_2$  and vacuum the oscillation parameters  $\phi$  and  $\theta_{12}$ . We present these expressions in Appendix B.

In terms of  $\tilde{\mathbf{D}}$  functions (45), the expressions for probabilities are similar to those for 1 layer (27)–(29) with, however, certain differences. Using (40)–(43) and definitions (45), we obtain

$$P(\nu_e \rightarrow \nu_e) = c_{13}^4(1 - \tilde{P}) + s_{13}^4, \quad (46)$$

$$\begin{aligned}P(\nu_\mu \rightarrow \nu_e) &= c_{13}^2 c_{23}^2 \tilde{P} - s_{13} c_{13}^2 \sin 2\theta_{23} \\ &\quad \times (\cos \delta R_{e\mu} + \sin \delta I_{e\mu}) \\ &\quad + s_{13}^2 c_{13}^2 s_{23}^2 (2 - \tilde{P}).\end{aligned}\quad (47)$$

Then

$$\begin{aligned}P(\nu_e \rightarrow \nu_\mu) &= c_{13}^2 c_{23}^2 \tilde{P} - s_{13} c_{13}^2 \sin 2\theta_{23} \\ &\quad \times (\cos \delta R_{\mu e} - \sin \delta I_{\mu e}) \\ &\quad + s_{13}^2 c_{13}^2 s_{23}^2 (2 - \tilde{P}).\end{aligned}\quad (48)$$

The most significant change is in the  $\nu_\mu \rightarrow \nu_\mu$  probability:

$$\begin{aligned}P(\nu_\mu \rightarrow \nu_\mu) &= 1 - 0.5 \sin^2 2\theta_{23} - c_{23}^4 \tilde{P} + s_{13} \sin 2\theta_{23} (c_{23}^2 - s_{13}^2 s_{23}^2) [\cos \delta (R_{e\mu} + R_{\mu e}) + \sin \delta (I_{e\mu} - I_{\mu e})] \\ &\quad + s_{13}^2 \sin^2 2\theta_{23} \frac{\tilde{P}}{2} \left\{ 1 + \frac{1}{\tilde{P}(1 - \tilde{P})} [\cos 2\delta (R_{e\mu} R_{\mu e} + I_{e\mu} I_{\mu e}) + \sin 2\delta (R_{\mu e} I_{e\mu} - R_{e\mu} I_{\mu e})] \right. \\ &\quad \left. + \frac{1}{\tilde{P}^2} (I_{e\mu} I_{\mu e} - R_{e\mu} R_{\mu e}) \right\} - 2s_{13}^2 s_{23}^4 + s_{13}^4 s_{23}^4 (2 - \tilde{P}).\end{aligned}\quad (49)$$

In the limit  $\phi \rightarrow 0$  (no oscillations in the atmosphere), we have

$$R_{e\mu} = R_{\mu e} = R_2, \quad I_{e\mu} = I_{\mu e} = I_2, \quad \tilde{P} = P_2, \quad (50)$$

and the formulas (46)–(49) are reduced to the one-layer formulas of the previous section. Notice that the functional dependence of the probabilities on the parameters  $s_{13}$ ,  $\delta$  and  $\theta_{23}$  is practically the same as in the one-layer case.

Let us consider expressions for  $R_{e\mu}$ ,  $R_{\mu e}$ ,  $I_{e\mu}$ ,  $I_{\mu e}$ , and  $\tilde{P}$  in the constant density approximation (see Appendix C.) They can be presented in the following form:

$$\tilde{\mathbf{D}}_i^c = \mathbf{D}_i^c(\phi^m + \phi) + \sin \Delta\theta \chi_i(\theta_{12}^m, \theta_{12}), \quad (51)$$

where  $\Delta\theta \equiv \theta_{12}^m - \theta_{12}$ . So,  $\tilde{\mathbf{D}}_i^c$  can be written as the corresponding functions for one layer of matter with total phase  $\phi^m + \phi$  plus corrections related to the difference of mixing angles in matter and vacuum. Since at low energies  $\Delta\theta \ll \theta_{12}$ , the second term in (51) can be considered as a small correction. In the first order in  $\Delta\theta$ , the expressions (C8) become

$$\begin{aligned}\tilde{P}^c &\approx \sin^2 2\theta_{12}^m \sin^2(\phi^m + \phi) - 2\Delta\theta \sin 4\theta_{12} \sin(\phi^m + \phi) \sin \phi \cos \phi^m, \\ R_{e\mu}^c &\approx -\frac{1}{2} \sin 4\theta_{12}^m \sin^2(\phi^m + \phi) + \Delta\theta [-\sin^2 2\theta_{12}^m \sin 2\phi \sin 2\phi^m + 2\sin^2 \phi (\cos 4\theta_{12} \cos^2 \phi^m + \sin^2 \phi^m)], \\ R_{\mu e}^c &\approx -\frac{1}{2} \sin 4\theta_{12}^m \sin^2(\phi^m + \phi) + \Delta\theta [\cos^2 2\theta_{12}^m \sin 2\phi \sin 2\phi^m + 2\sin^2 \phi (\cos 4\theta_{12} \cos^2 \phi^m - \sin^2 \phi^m)], \\ I_{e\mu}^c &\approx \frac{1}{2} \sin 2\theta_{12}^m \sin 2(\phi^m + \phi) - \Delta\theta \cos 2\theta_{12}^m \sin 2\phi, \\ I_{\mu e}^c &\approx \frac{1}{2} \sin 2\theta_{12}^m \sin 2(\phi^m + \phi) + \Delta\theta \cos 2\theta_{12}^m [-\sin 2\phi \cos 2\phi^m + 2\sin^2 \phi \sin 2\phi^m].\end{aligned}\quad (52)$$

At energies  $E < 60$  MeV the magnitude of second term does not exceed 0.1. For high energies the difference  $\Delta\theta$  becomes large. However, in this case the oscillation length increases and  $\phi$  becomes smaller, so that the oscillations in the atmosphere can be neglected.

In summary, final expressions for the flavor probabilities are given in Eqs. (46)–(49) with  $\tilde{P}$ ,  $R_{e\mu}$ ,  $I_{e\mu}$ ,  $R_{\mu e}$ , and  $I_{\mu e}$  as functions of  $P_2$ ,  $R_2$ , and  $I_2$ , and the vacuum oscillation parameters are presented in Appendix B. In turn, the precise semianalytical expressions for  $P_2$ ,  $R_2$ , and  $I_2$  are

given in (35) for the first order Magnus expansion and in Appendix A for the second order.

## V. AVERAGING OF OSCILLATIONS AND INTEGRATION OVER THE ZENITH ANGLE

Results for the oscillation probabilities obtained in the previous section are simplified substantially after integration over the zenith angle. In what follows, we will consider detection of neutrinos by the charged current

interactions with nucleons, where the information about neutrino direction is essentially lost. Consequently, observables (at least in the first approximation) are given by integration over the zenith angle. To a good approximation, the neutrino flux at low energies does not depend on the zenith angle  $\Theta_\nu$ , and therefore integration over the angle is reduced to averaging of probabilities over  $\Theta_\nu$ .

In the constant density approximation, the probabilities averaged over the oscillation phase equal

$$\langle P_2^c \rangle_\phi = \frac{1}{2} \sin^2 2\theta_{12}^m, \quad \langle R_2^c \rangle_\phi = -\frac{1}{4} \sin 4\theta_{12}^m, \quad \langle I_2^c \rangle_\phi = 0, \quad (53)$$

where the subscript means averaging over the phase. For antineutrinos one should substitute  $\theta_{12}^m \rightarrow \bar{\theta}_{12}^m$ . As a consequence of  $I_2^c = 0$ , the  $CP$ -odd terms of probabilities (which lead to the  $CP$  asymmetries) become zero, as is expected, since this would correspond to averaging over all oscillation phases (we have already averaged over the 1-3 phase). The real part  $R_2$  determines the first order correction due to the 1-3 mixing.

For very low energies we have  $\theta_{12}^m \approx \theta_{12}$ , and, consequently,  $\langle R_2 \rangle_\phi = \langle \bar{R}_2 \rangle_\phi = -\frac{1}{4} \sin 4\theta_{12} \approx -0.19$ . For antineutrinos with an increase of energy, the angle  $\bar{\theta}_{12}^m$  decreases. As a result,  $\langle \bar{R}_2 \rangle_\phi < 0$  in the whole energy range. The absolute value  $|\langle \bar{R}_2 \rangle_\phi|$  first increases, reaches maximal value 0.25 when  $\bar{\theta}_{12}^m = 22.5^\circ$  (at  $E \sim 150$  MeV), and then decreases. In contrast, the angle  $\theta_{12}^m$  increases, and therefore  $\langle R_2 \rangle_\phi$  first decreases, becomes zero in the resonance ( $E \sim 100$  MeV), and then changes sign:  $\langle R_2 \rangle_\phi > 0$ . It increases with energy until  $E \sim 300$  MeV and then decreases again.

For the two-layer case, we obtain after averaging over the phases

$$\begin{aligned} \langle \tilde{P}^c \rangle_\phi &= \frac{1}{2} \sin^2 2\theta_{12}^m - \frac{1}{4} (\sin^2 2\theta_{12}^m - \sin^2 2\theta_{12}) \\ &\quad + \frac{1}{4} \sin^2 2(\theta_{12} - \theta_{12}^m), \\ \langle R_{e\mu}^c \rangle_\phi &= -\frac{1}{4} \sin 4\theta_{12}^m + \frac{1}{8} [\sin 4\theta_{12}^m - \sin 4\theta_{12} \\ &\quad + \sin 4(\theta_{12}^m - \theta_{12})], \\ \langle R_{\mu e}^c \rangle_\phi &= -\frac{1}{4} \sin 4\theta_{12}^m + \frac{1}{8} [\sin 4\theta_{12}^m - \sin 4\theta_{12} \\ &\quad - \sin 4(\theta_{12}^m - \theta_{12})], \\ \langle I_{e\mu}^c \rangle_\phi &= \langle I_{\mu e}^c \rangle_\phi = 0. \end{aligned} \quad (54)$$

At very low energies, when the difference of mixing angles in vacuum and in matter is very small, we find from (54):

$$\begin{aligned} \langle \tilde{P} \rangle_\phi &\approx \frac{1}{2} \sin^2 2\theta_{12}^m - \frac{1}{2} \Delta\theta \sin 4\theta_{12}, \\ \langle R_{e\mu} \rangle_\phi &= -\frac{1}{2} \sin 4\theta_{12}^m + \Delta\theta \cos^2 2\theta_{12}, \\ \langle R_{\mu e} \rangle_\phi &= -\frac{1}{2} \sin 4\theta_{12}^m - \Delta\theta \sin^2 2\theta_{12}. \end{aligned} \quad (55)$$

These averaged functions  $\langle D_i \rangle_\phi$  determine the number of low energy events. Indeed, to find the number of events we need to integrate the probabilities folded with the

neutrino fluxes and cross sections over the zenith angle  $\Theta_\nu$  (the angular variables, in general). In turn, the oscillation probabilities are linear functions of  $\tilde{\mathbf{D}}_i$ . Therefore we deal here with integrals

$$J_i = \int d(\cos\Theta_\nu) \tilde{D}_i(\cos\Theta_\nu) F(\Theta_\nu). \quad (56)$$

At low energies the fluxes do not depend on  $\Theta_\nu$ , and, consequently,

$$J_i = 2F \langle \tilde{D}_i(\cos\Theta_\nu) \rangle. \quad (57)$$

Here  $\langle \dots \rangle$  without a subscript denotes averaging over the zenith angle  $\Theta_\nu$ . The functions  $D_i$  depend on  $\cos\Theta_\nu$  via the oscillation phases  $\phi$  and  $\phi_m$ . Apparently,  $\phi \propto L_A(\cos\Theta_\nu)$ , and in the constant density approximation,  $\phi_m \propto L_m \propto \cos\Theta_\nu$ . Therefore averaging over  $\cos\Theta_\nu$  is equivalent to averaging over the phase  $\phi_m$  as we did above. The situation is different for the terms which depend on the vacuum phase. Indeed, according to (4) the dependence of  $\phi$  on  $\cos\Theta_\nu$  is nonlinear. In particular, for trajectories not very close to the horizon,  $L_A \propto 1/\cos\Theta_\nu$  and therefore integration over  $\cos\Theta_\nu$  is not reduced to averaging over the phase. For estimations, the effect of oscillations in the atmosphere can be taken into account by the additional factor  $\kappa$  as

$$\langle \tilde{D}_i(\cos\Theta_\nu) \rangle \approx \frac{1}{2} \int d(\cos\Theta_\nu) \tilde{D}_i = \frac{\kappa}{2} \langle \tilde{D}_i \rangle_\phi, \quad (58)$$

where  $\langle D_i \rangle_\phi$  refers to averaging over the phase. The factor  $\kappa$  equals 1, if oscillations in the atmosphere can be neglected. For low energy bins ( $E < 15$  MeV)  $\kappa$  can be as big as 1.2; for  $E = 20$  MeV we have  $\kappa \sim 1.1$  and  $\kappa$  approaches 1 with an increase of energy.

## VI. NEUTRINO FLUXES AT THE DETECTOR

The  $\nu_e$  flux at the detector with oscillations taken into account,  $F_e$ , can be written as

$$\begin{aligned} F_e &= F_e^0 P(\nu_e \rightarrow \nu_e) + F_\mu^0 P(\nu_\mu \rightarrow \nu_e) \\ &= F_e^0 [P(\nu_e \rightarrow \nu_e) + r P(\nu_\mu \rightarrow \nu_e)], \end{aligned} \quad (59)$$

where  $r$  is defined in (1). For antineutrinos we have a similar expression with substitutions  $P \rightarrow \bar{P}$ ,  $F \rightarrow \bar{F}$ , and  $r \rightarrow \bar{r}$ .

Inserting the probabilities  $P_{ee}$  and  $P_{\mu e}$  from (46) and (47) into (59), we obtain the expression for the relative change of the  $\nu_e$  flux due to oscillations:

$$\begin{aligned} \frac{F_e}{F_e^0} &= 1 + (rc_{23}^2 - 1)\tilde{P} - rs_{13}c_{13}^2 \sin 2\theta_{23} (\cos \delta R_{e\mu} \\ &\quad + \sin \delta I_{e\mu}) - 2s_{13}^2 [(1 - rs_{23}^2) + \tilde{P}(r - 2)] \\ &\quad + s_{13}^4 (1 - rs_{23}^2)(2 - \tilde{P}). \end{aligned} \quad (60)$$

It coincides (up to the sign of  $\delta$  and the corresponding change of  $\mathbf{D} \rightarrow \tilde{\mathbf{D}}$ ) with the expression in our previous paper [14]. Notice that the corrections of the order  $s_{13}^2$



are suppressed by the ‘‘screening’’ factors which are zero for maximal 2-3 mixing and  $r = 2$ . There are no corrections of the order  $s_{13}^3$ .

The  $\nu_\mu$  flux at the detector with oscillations taken into account,  $F_\mu$ , can be written as

$$\begin{aligned} F_\mu &= F_\mu^0 P(\nu_\mu \rightarrow \nu_\mu) + F_e^0 P(\nu_e \rightarrow \nu_\mu) \\ &= F_\mu^0 \left[ P(\nu_\mu \rightarrow \nu_\mu) + \frac{1}{r} P(\nu_e \rightarrow \nu_\mu) \right]. \end{aligned} \quad (61)$$

Then the ratio of fluxes with and without oscillations equals

$$\begin{aligned} \frac{F_\mu}{F_\mu^0} &= 1 - \frac{1}{2} \sin^2 2\theta_{23} - c_{23}^2 \tilde{P} \left( c_{23}^2 - \frac{c_{13}^2}{r} \right) \\ &\quad - s_{13} \sin 2\theta_{23} \left\{ \cos \delta \left[ \frac{R_{\mu e}}{r} - c_{23}^2 (R_{e\mu} + R_{\mu e}) \right] \right. \\ &\quad \left. - \sin \delta \left[ \frac{I_{\mu e}}{r} + c_{23}^2 (I_{e\mu} + I_{\mu e}) \right] \right\} + O(s_{13}^2). \end{aligned} \quad (62)$$

Averaging over the zenith angle vanishes the imaginary parts. Notice that the linear in  $s_{13}$  term is proportional to  $R_{e\mu} + R_{\mu e} \approx 2R_2$ .

## VII. ELECTRON NEUTRINO (ANTINEUTRINO) EVENTS

We will discuss here (mostly for illustration) a detection of the low energy neutrinos in the water Cherenkov detectors. In these detectors the electron neutrinos are detected via the quasielastic scattering

$$\begin{aligned} \bar{\nu}_e + p &\rightarrow e^+ + n, & \bar{\nu}_e + {}^{16}\text{O} &\rightarrow e^+ + N, \\ \nu_e + {}^{16}\text{O} &\rightarrow e^- + F. \end{aligned} \quad (63)$$

The energy of the positron (electron) is practically uniquely related to the neutrino energy:  $E_e = E_\nu - 1.293$  MeV (for  ${}^1\text{H}$ ) and  $E_e = E_\nu - 15$  MeV (for  ${}^{16}\text{O}$ ). The number of  $e^+$  events (63) has been computed as

$$\begin{aligned} N_{\bar{e}} &\propto \sum_{i=p,O} \int dE_\nu dE_e d(\cos\Theta_\nu) F_{\bar{e}}(E_\nu, \Theta_\nu) \\ &\quad \times \frac{d\sigma_i}{dE_e} \Psi(\Theta_e, \Theta_\nu, E_\nu) \varepsilon(E_e), \end{aligned} \quad (64)$$

where  $F_{\bar{e}}$  is the atmospheric  $\bar{\nu}_e$  flux at the detector given in (60) for  $\bar{\nu}_e$ ; the fluxes  $F_e^0$  and  $F_\mu^0$  without oscillations are taken from Refs. [3,4,6];  $d\sigma_i/dE_e$  are the differential cross sections [16];  $\varepsilon(E_e)$  is the detection efficiency.  $\Psi$  is the ‘‘dispersion’’ function which describes deviation of the lepton zenith angle from the neutrino zenith angle (for details, see Ref. [17]). Summation proceeds over scattering on hydrogen and oxygen. For  $\nu_e$  we use a similar expression for a number of events but consider the reaction on oxygen only.

Results of computations of the energy spectra of  $\bar{\nu}_e$  and  $\nu_e$  events for different values of 2-3 mixing are shown in Fig. 4. Qualitative and to a large extent quantitative understanding of these results can be obtained from the following semianalytical consideration. The number of events can be presented as

$$N_e = \left\langle \frac{F_e}{F_e^0} \right\rangle N_e^0, \quad (65)$$

where  $N_e^0$  is the number of events without oscillations; the ratio of fluxes  $F_e/F_e^0$  is given in (60), and averaging proceeds over the neutrino energy bin and the zenith angle.

The relative change of the spectrum can be written in the following way:

$$\frac{N_e}{N_e^0} = 1 + \epsilon_e^{(0)} + \epsilon_e^{(1)} + \epsilon_e^{(2)} + \dots, \quad (66)$$

where

$$\epsilon_e^{(0)} = \langle \tilde{P}(E) \rangle [ \langle r(E) \rangle c_{23}^2 - 1 ] \quad (67)$$

is the correction due to the oscillations driven by the 1-2 mixing and split for  $s_{13} = 0$ ;

$$\epsilon_e^{(1)} = -s_{13} \cos \delta \sin 2\theta_{23} \langle r \rangle \langle R_{e\mu} \rangle \quad (68)$$

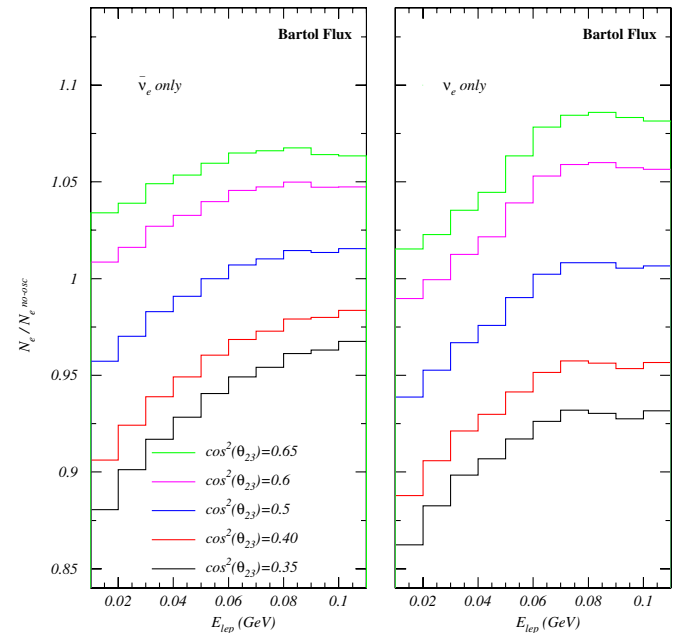


FIG. 4 (color online). Left panel: Distortion of the positron energy spectrum due to oscillations of the atmospheric  $\bar{\nu}_e$ . Shown is the ratio  $N_e/N_e^0$  as a function of the positron energy for different values of  $\cos^2\theta_{23}$ . The Bartol fluxes and values of oscillation parameters  $\sin^2 2\theta_{12} = 0.82$ ,  $\Delta m_{21}^2 = 7.3 \times 10^{-5} \text{ eV}^2$ , and  $s_{13} = 0$  were used for calculations of the histograms. Both interactions with  ${}^1\text{H}$  and  ${}^{16}\text{O}$  in a water Cherenkov detector are taken into account. Right panel: The same as in the left panel for the atmospheric  $\nu_e$  and the electron spectrum. The interactions with  ${}^{16}\text{O}$  in water Cherenkov detectors are taken into account.

is the first linear correction due to 1-3 mixing, etc. Here  $\langle \bar{P}(E) \rangle$ ,  $\langle R_{e\mu}(E) \rangle$ , and  $\langle r(E) \rangle$  are the probabilities and the ratio of fluxes averaged over the zenith angle and energy bin, correspondingly. We take  $\langle rR_2 \rangle \approx \langle r \rangle \langle R_2 \rangle$ . For antineutrinos,  $P_2 \rightarrow \bar{P}_2(E)$  and  $r \rightarrow \bar{r}$ .

In Fig. 4 (left panel), we show distortion of the energy spectrum of positrons produced by the atmospheric  $\bar{\nu}_e$  for  $s_{13} = 0$ . All of the features of the curves can be traced from Eqs. (66) and (67). The averaged probability  $\langle \bar{P}_2(E) \rangle$  slightly decreases with energy. For estimations one can use the oscillation probability for a layer of constant density, so that  $\langle \bar{P}_2(E) \rangle \sim 0.25\kappa \sin^2 2\theta_m$ , where  $\kappa$  takes into account oscillations in the atmosphere (58).

For the antineutrino channel,  $\sin^2 2\theta_m$  decreases with an increase of energy. Estimations give  $\langle P_2(E) \rangle = 0.089$ , 0.038, and 0.013 for  $E = 20, 40$ , and 80 MeV, correspondingly. For a given  $c_{23}^2$ , the change of  $\epsilon_{\bar{e}}^{(0)}$  reflects this decrease of  $\langle \bar{P}_2(E) \rangle$  and change of  $\langle \bar{r}(E) \rangle$ . In general,  $\epsilon_{\bar{e}}^{(0)}$  decreases with energy. Distortion of spectrum can be characterized by  $\Delta\epsilon_{\bar{e}}^{(0)} \equiv \epsilon_{\bar{e}}(100 \text{ MeV}) - \epsilon_{\bar{e}}(10 \text{ MeV})$ . According to the figure, the distortion  $\Delta\epsilon_{\bar{e}}^{(0)}$  is stronger for small  $c_{23}^2$ ; it decreases from  $\sim(8-9)\%$  for  $c_{23}^2 = 0.35$  down to  $\sim(2-3)\%$  for  $c_{23}^2 = 0.65$ . Thus, if the shape of spectrum can be predicted with accuracy  $\sim 1\%$ , one can measure the deviation of 2-3 mixing from maximal by studying the distortion of the spectrum in a way which does not depend on uncertainties of the absolute value of neutrino flux. One possibility is to compare the integrated signal below and above 53 MeV.

For  $c_{23}^2 > 0.6$  the dependence is not monotonous: With a decrease of  $E$ ,  $\epsilon_{\bar{e}}$  first increases and then decreases. For  $c_{23}^2 > 0.6$  the oscillation effect is positive  $\epsilon_{\bar{e}} > 0$  in the whole energy range, whereas for  $c_{23}^2 < 0.42$ ,  $\epsilon_{\bar{e}}^{(0)} < 0$  everywhere, and for  $c_{23}^2 \sim 0.5$  the correction  $\epsilon_{\bar{e}}^0$  changes the sign.

With a change of  $c_{23}^2$ ,  $\Delta\epsilon_{\bar{e}}^{(0)} = \epsilon_{\bar{e}}(0.65) - \epsilon_{\bar{e}}(0.35) = (11-12)\%$  for large energies ( $E \sim 90$  MeV), and  $\Delta\epsilon_{\bar{e}} = 16\%$  in the low energy bin. So, if the absolute flux is known with accuracy of a few percent, the 2-3 mixing can be determined by just measuring the total number of events. Variation of the signal with  $c_{23}^2$  is stronger here than in the sub-GeV sample ( $E > 100$  MeV), although the number of events is smaller.

In Fig. 4 (right panel), we show the distortion of spectrum of the  $e$ -like events induced by scattering of  $\nu_e$  on  $^{16}\text{O}$ . For neutrinos the flavor ratio  $r$  is systematically smaller than for antineutrinos. Therefore the histograms shift to smaller values of ratio  $N_e/N_e^0$ . The suppression of signal due to oscillations is stronger here. A character of the distortion is rather similar to that in the  $\bar{\nu}$  case, and, again, it can be traced from Eqs. (66) and (67). Now  $\langle P_2(E) \rangle$  changes with energy weaker. Indeed,  $\kappa$  decreases, whereas  $\sin^2 2\theta_m$  increases with the energy increase, and the two changes partly compensate each other. For a given

$c_{23}^2$  we obtain  $\Delta\epsilon_e^{(0)} \equiv \epsilon_e^{(0)}(100 \text{ MeV}) - \epsilon_e^{(0)}(10 \text{ MeV}) \sim 6\%$  for all values of  $c_{23}^2$  in the interval 0.35–0.65. For fixed energy, with a change of  $c_{23}^2$  one has  $\epsilon_e^{(0)}(0.35) - \epsilon_e^{(0)}(0.65) \sim 15\%$  for all energies.

In Fig. 5, we compare the distortions of spectra of events computed with the neutrino fluxes published by different authors. This quantifies the present theoretical uncertainties. Fluxes from [4] (Honda) and [3] (Bartol) lead to a rather similar distortion although according to [4]  $r(E)$  is flatter than in [3] in the range  $E > 60$  MeV, but below that energy  $r(E)$  decreases sharper (see Fig. 2). For large  $c_{23}^2$  this leads to a nonmonotonous change of  $\epsilon_{\bar{e}}$  with maximum at  $E = (60-70)$  MeV, as we have marked before.

Corrections due to 1-3 mixing described by  $\epsilon_e^{(1)} + \epsilon_e^{(2)} + \dots$  are shown in Fig. 6 for antineutrinos (left panel) and for neutrinos (right panel). All of the features of the figures can be immediately understood using the analytic expressions derived above. Recall that due to integration over the zenith angle  $I_2$  becomes negligible [see Eq. (53)]. Moreover, as we marked before, the corrections of the order  $s_{13}^2$  are additionally suppressed. Therefore in the first approximation the corrections are given by  $\epsilon_e^{(1)}$  in Eq. (68). This term weakly depends on  $\theta_{23}$ .  $\langle R_{e\mu} \rangle$  can be estimated by taking the constant density approximation:

$$\langle R_{e\mu} \rangle \approx \langle R_2 \rangle \sim -\frac{\kappa}{8} \sin 4\theta_{12}^m. \quad (69)$$

For directions below the horizon, the corrections due to oscillations in the atmosphere are additionally suppressed by  $\cos^2 2\theta_{12} \approx 0.18$  (55).

Consider first the effect for antineutrinos. In the lowest energy bin we have  $\langle \bar{r} \rangle = 1.7$ ,  $\kappa \sim 1.2$ , and  $\langle \bar{R}_{e\mu} \rangle = -0.085\kappa$ . Therefore the linear in  $s_{13}$  correction equals

$$\epsilon_{\bar{e}}^{(1)}(10 \text{ MeV}) \approx 0.021 \left( \frac{s_{13} \cos \delta}{0.126} \right). \quad (70)$$

With an increase of energy, both  $\langle \bar{R}_2 \rangle$  and  $\langle \bar{r} \rangle$  increase, and at  $E = 100$  MeV ( $0.5 \sin 4\theta_{12}^m \approx 0.48$ )

$$\epsilon_{\bar{e}}^{(1)}(100 \text{ MeV}) \approx 0.033 \left( \frac{s_{13} \cos \delta}{0.126} \right) \quad (71)$$

in agreement with the results in Fig. 6. The corrections are  $CP$ -even being of the same sign for neutrinos and antineutrinos.

For neutrinos we have  $\langle r \rangle = 1.66$  in the lowest energy bin, and, consequently,

$$\epsilon_e^{(1)}(10 \text{ MeV}) \approx 0.025 \left( \frac{s_{13} \cos \delta}{0.126} \right). \quad (72)$$

The correction decreases with energy due to a decrease of  $\langle R_{e\mu} \rangle$ . For  $E = 60$  MeV we have  $\langle r \rangle = 2.0$ ,  $\langle R_{e\mu} \rangle = -0.035$ , and therefore

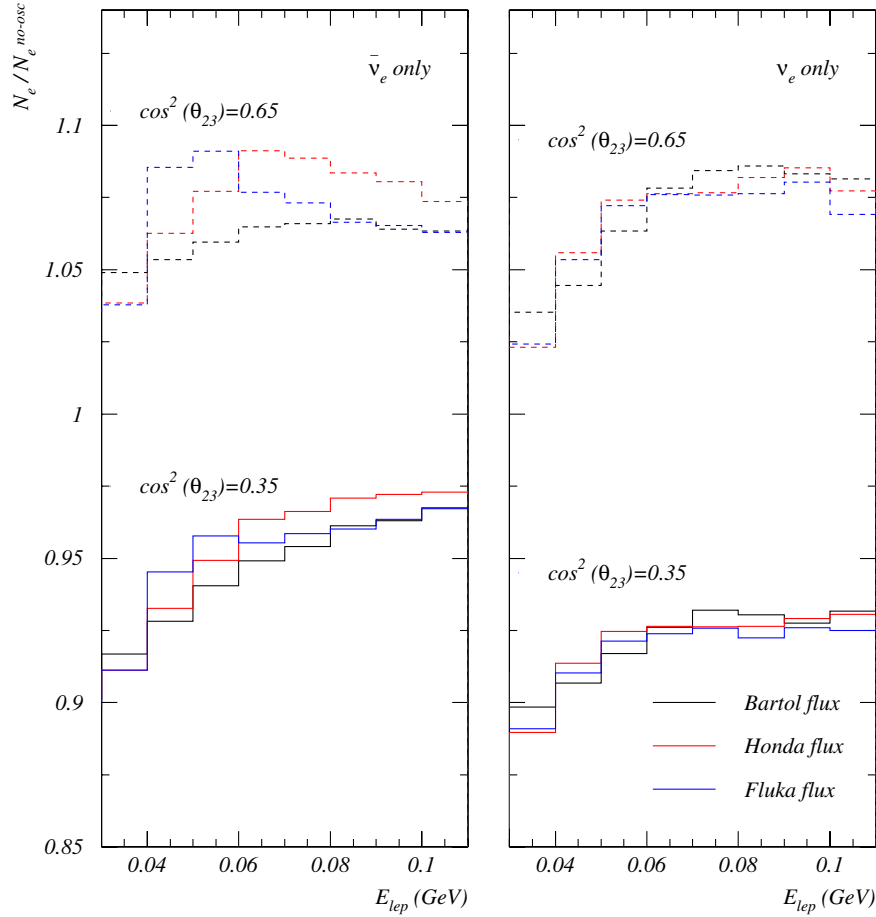


FIG. 5 (color online). Distortions of the energy spectra of events for the neutrino fluxes from different computations. The full and dashed lines correspond to two different values of  $\cos^2\theta_{23}$ . Left panel:  $\bar{\nu}_e$ . Right panel:  $\nu_e$ .

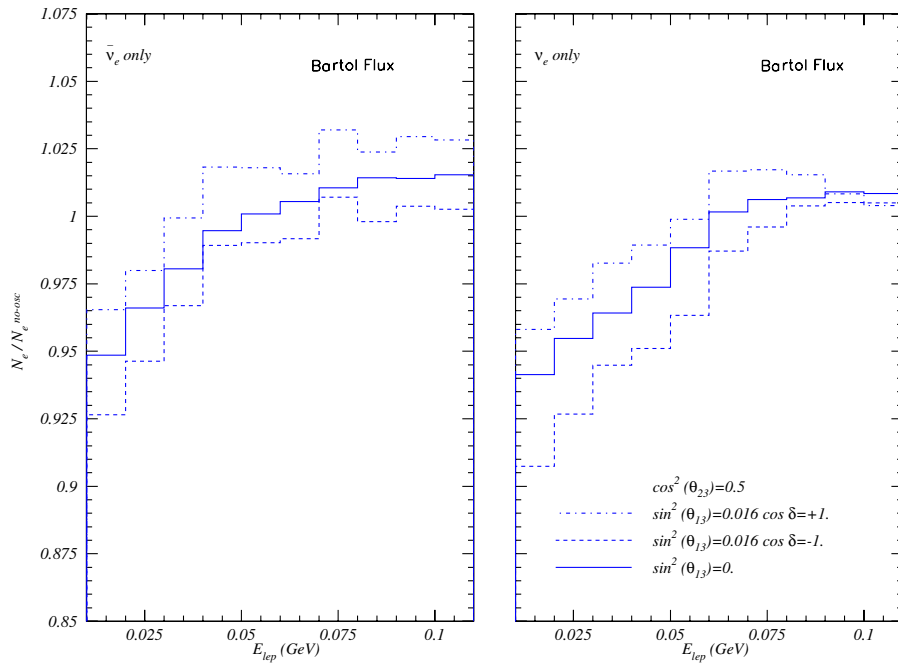


FIG. 6 (color online). Effect of the 1-3 mixing on the spectra of events induced by the electron neutrinos and antineutrinos. Shown are relative spectra of the  $e$ -like events for different values of 1-3 mixing. We take  $c_{23}^2 = 0.5$ ,  $\sin^2 2\theta_{12} = 0.82$ , and  $\Delta m_{21}^2 = 7.3 \times 10^{-5} \text{ eV}^2$ . Left panel:  $\bar{\nu}_e$ . Right panel:  $\nu_e$ .

$$\epsilon_e^{(1)}(60 \text{ MeV}) \approx 0.009 \left( \frac{s_{13} \cos \delta}{0.126} \right). \quad (73)$$

In the resonance  $R_{e\mu} \approx 0$ . Therefore, in the region around  $E \sim 90$  MeV, the corrections due to 1-3 mixing are suppressed additionally, as can be seen from Fig. 6.

Comparing results from different energy regions, we can identify the 1-3 mixing effect (induced interference). Notice that corrections due to 1-3 mixing weakly depend on the 2-3 mixing which allows us to disentangle the effect of 1-3 mixing  $\epsilon_e^{(1)}$  and the effect due to the 1-2 mixing which is proportional to the deviation of 2-3 mixing from maximal.

Corrections proportional to  $s_{13}^2$ ,

$$\epsilon_e^{(2)} \sim 2s_{13}^2 [(\langle r \rangle s_{23}^2 - 1) + \langle \tilde{P} \rangle (2 - \langle r \rangle)], \quad (74)$$

are small:  $<0.005$  for  $s_{13}^2 = 0.016$ . Thus, the degeneracy of  $s_{13}^2$  and  $c_{23}^2$  parameters can, in principle, be resolved using the energy dependence of the effect for neutrinos; however, for antineutrinos the energy dependence is weak.

### VIII. MUON NEUTRINO DETECTION: INVISIBLE MUON DECAYS

Muon neutrinos can be observed via the decay of invisible muons. Muons with energies below 160 MeV do not

produce a signal in water Cherenkov detectors. They quickly lose energy, stop, and decay at rest emitting an electron (positron). In turn, most of these muons are produced in the detector in the quasielastic interactions  $\nu_\mu + N \rightarrow N' + \mu$ . The effective (reconstructed) energy spectrum of these neutrinos has a maximum at 0.16 GeV and extends to 0.25 GeV [8]. In this energy range  $F_\mu \approx F_{\bar{\mu}}$ ,  $F_e > F_{\bar{e}}$ , and the flavor ratios equal  $r = 2.03$  and  $\bar{r} = 2.23$  [6]. Typical energies of neutrinos are high enough so that for estimations we can neglect the oscillations in the atmosphere and use functions **D**.

Consider effects of oscillations on the number of electrons/positrons from invisible muon decay. Apparently, the shape of the energy spectrum of events is not influenced by oscillations, and it has the standard form with a maximum at 45 MeV.

In Fig. 7, we show the ratio of the number of the invisible muon decays with and without oscillations  $N_\mu/N_\mu^0$  as a function of  $c_{23}^2$  for different values of  $s_{13}$ . All of the features of this figure can be traced from the following semianalytic consideration. According to (62) we have approximately

$$\frac{N_\mu}{N_\mu^0} \sim 1 - \frac{1}{2} \sin^2 2\theta_{23} + \epsilon_\mu^{(0)} + \epsilon_\mu^{(1)} + \epsilon_\mu^{(2)} + \dots \quad (75)$$

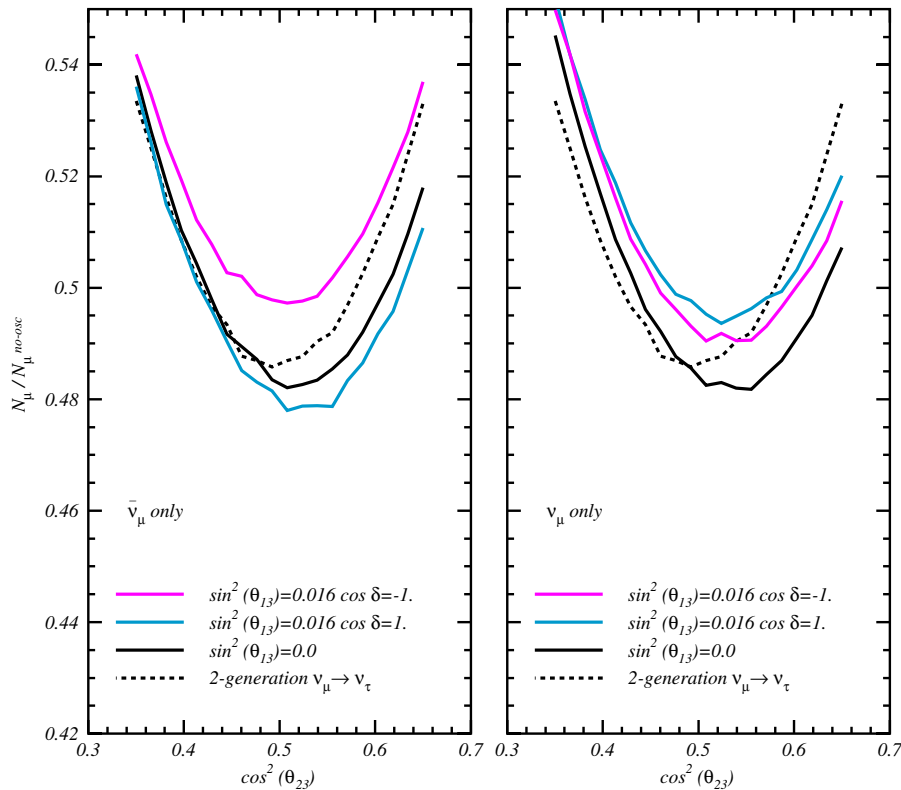


FIG. 7 (color online). Oscillation effects on the total number of invisible  $\mu$ -decay events induced by antineutrinos (left panel) and neutrinos (right panel). Shown is the dependence of  $N_\mu/N_\mu^0$  on  $c_{23}^2$  for different values of 1-3 mixing. The dashed line corresponds to the vacuum  $\nu_\mu - \nu_\tau$  oscillations (zero 1-2 and 1-3 mixings).

The zero order (in  $s_{13}$ ) correction equals

$$\epsilon_{\mu}^{(0)} \approx -\langle P_2 \rangle c_{23}^2 \left( c_{23}^2 - \frac{1}{\langle r \rangle} \right). \quad (76)$$

The linear in  $s_{13}$  correction is given by

$$\epsilon_{\mu}^{(1)} \approx s_{13} \sin 2\theta_{23} \cos \delta \langle R_2 \rangle \left( 2c_{23}^2 - \frac{1}{\langle r \rangle} \right). \quad (77)$$

The quadratic in  $s_{13}$  corrections can be written as

$$\begin{aligned} \epsilon_{\mu}^{(2)} \approx s_{13}^2 \left[ \sin^2 2\theta_{23} \left[ \cos^2 \delta \langle P_2 \rangle + \frac{1}{2} \left\langle \frac{I_2^2 - R_2^2}{P_2} \right\rangle \right] \right. \\ \left. - 2s_{23}^4 + \frac{1}{\langle r \rangle} (2s_{23}^2 - \langle P_2 \rangle) \right]. \quad (78) \end{aligned}$$

In the constant density approximation we have

$$\frac{I_2^2 - R_2^2}{P_2} = 1 - (1 + \cos^2 2\theta_{12}^m) \sin^2 \phi^m, \quad (79)$$

and averaging over the zenith angle gives

$$\left\langle \frac{I_2^2 - R_2^2}{P_2} \right\rangle = \frac{1}{2} \left( 1 + \frac{1}{2} \sin^2 2\theta_{12}^m \right). \quad (80)$$

The first term in (75) is just the averaged vacuum  $\nu_{\mu} - \nu_{\tau}$  oscillation probability. This probability (black curve) is symmetric with respect to maximal mixing:  $c_{23}^2 = 0.5$ . As expected, at this value of  $c_{23}^2$  one has maximal suppression 0.5.

Corrections due to the oscillations driven by the 1-2 mixing  $\epsilon_{\mu}^{(0)}$  are asymmetric with respect to  $c_{23}^2 = 0.5$ . The corrections are zero at  $c_{23}^2 = 1/\langle r \rangle$ . They are positive at smaller  $c_{23}^2$  and negative at  $c_{23}^2 > 1/\langle r \rangle$ . The maximal relative effect is  $\approx 5\%$  suppression at  $c_{23}^2 = 0.65$ . The effect is weaker ( $< 3\%$ ) for antineutrinos which is related to smaller probability  $\bar{P}_2$ , and a larger value of  $\bar{r}$  only partly compensates the difference.

The first order correction due to the 1-3 mixing  $\epsilon_{\mu}^{(1)}$  is given in (77). For the average energy of neutrinos producing invisible muons  $E = 160$  MeV, we have  $\langle R_2 \rangle = 0.04$  and  $\langle \bar{R}_2 \rangle = -0.125$ . Notice that the energies of neutrinos which generate the invisible muons are above the resonance, and therefore  $R_2$  has sign opposite to  $\bar{R}_2$ . Then for  $c_{23}^2 = 0.65$  we obtain

$$\epsilon_{\mu}^{(1)} \approx 0.004 \left( \frac{s_{13} \cos \delta}{0.126} \right). \quad (81)$$

For antineutrinos the corrections are much larger and of opposite sign:

$$\epsilon_{\mu}^{(1)} \approx -0.0127 \left( \frac{s_{13} \cos \delta}{0.126} \right). \quad (82)$$

This is in agreement with the results of Fig. 7.

In contrast to the direct  $\nu_e$  channel, here  $s_{13}^2$  corrections are not suppressed by the screening factors and turn out to

be of the same order as the linear corrections for not too small  $s_{13}^2$ . Using (78) we get for the quadratic term and  $\cos \delta = 1$

$$\epsilon_{\mu}^{(2)} \approx 0.0085 \left( \frac{s_{13}^2}{0.016} \right), \quad (83)$$

and for antineutrinos the corresponding numerical coefficient equals 0.0054. The corrections are positive.

Notice that the high energy neutrino fluxes responsible for the invisible muon production are affected by the solar activity weaker than fluxes at low energies. At  $E > 150$  MeV the difference of fluxes during minimum and maximum of solar activity is (6–10)%, whereas at 30 MeV the difference is about 24%. Variations at high energies are weaker. This can be used to disentangle the direct production and signal from the invisible muon decays.

## IX. FUTURE MEASUREMENTS

High statistics of the sub-sub-GeV events can be obtained in future megaton-scale water Cherenkov detectors [18–21]. In these detectors the signals of four different neutrino fluxes considered in the previous sections can be identified in the following way:

- (1) The  $\bar{\nu}_e$  quasielastic scattering on protons can be detected performing tagging of neutrons in correlation to the positron detection. In SuperKamiokande this will be possible with gadolinium in the way proposed in Ref. [22].
- (2) The  $\bar{\nu}_\mu$  quasielastic scattering on protons has similar signatures: detection of neutron and positron from the muon decay. The difference from the previous case is that positrons appear in a certain energy range and have a known energy spectrum. So the number of invisible decays can be extracted by fitting the energy spectrum. (Also, neutrons will have different energy characteristics.)
- (3) The electron neutrinos  $\nu_e$ 's are detected by their scattering on oxygen. An electron appearing in this process should not be accompanied by a neutron. (In principle, one can perform tagging of nuclear transitions, e.g., detecting transition to an excited state of nuclei.)
- (4) The  $\nu_\mu$  flux is detected via the invisible muon production on oxygen. The standard decay spectrum of electrons and absence on neutron are the signatures of this interaction.

Thus, the antineutrino-induced events can be disentangled from neutrino interactions by the neutron tagging.

Certain conclusions can be drawn from comparison of different signals. The oscillation corrections to the  $\nu_e$  signal are substantially enhanced in comparison to the  $\bar{\nu}_e$  corrections if  $c_{23}^2 < 0.5$ . Comparison of the  $\nu_e$  and  $\bar{\nu}_e$  signals at  $E > 60$  MeV can reveal the effect of 1-3 mixing.

Figure 8 illustrates dependence of the spectra of the  $e$ -like events on the 2-3 mixing for  $s_{13} = 0$ . The histograms show spectra of the  $e$ -like events produced directly by the electron neutrinos and antineutrinos (red and blue) and from the invisible muon decay (black) for different values of  $\cos\theta_{23}$ . We show the number of  $e$ -like events at HyperKamiokande (540 kton collected during 4 years). The difference of numbers of events for  $c_{23}^2 = 0.35$  and  $c_{23}^2 = 0.65$  in each bin is about  $2\sigma$  (statistical error). Therefore using 9 bins one can distinguish two values of  $c_{23}^2$  at the  $18\sigma$  level.

The effect of 1-3 mixing is much stronger in the antineutrino signal than in the neutrino signal for both the electron and muon neutrinos (i.e., for both components shown in Fig. 9). The difference of histograms is essentially due to the linear  $s_{13}$  corrections. Qualitatively, the size of the effect can be immediately inferred from Eq. (68) for the direct component and from Eqs. (77), (81), and (82) for the invisible muon decays.

For maximal allowed value  $s_{13}^2 = 0.03$  one would get a 1.4 times larger difference of histograms than the one shown in Fig. 9.

Notice that with an increase of  $c_{23}^2$  the number of invisible  $\mu$  decays increases for  $c_{23}^2 > 0.5$  and decreases for

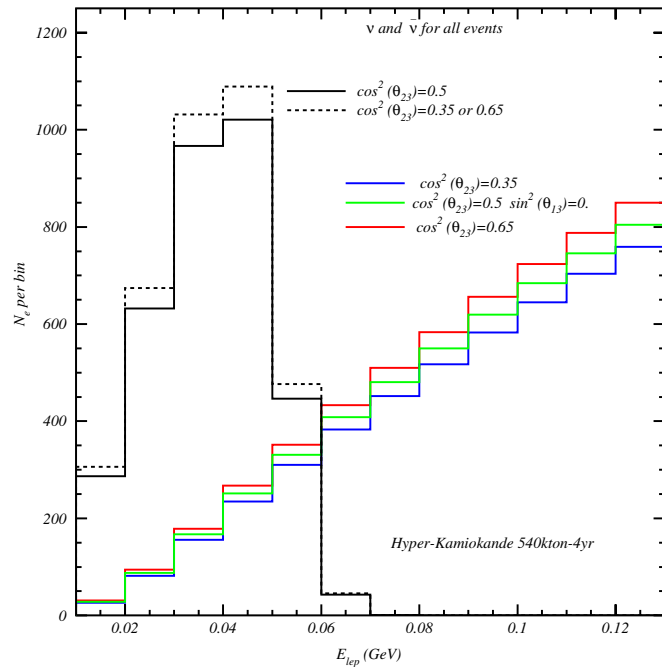


FIG. 8 (color online). The spectrum of neutrino and antineutrino events expected for 4 years of the HyperKamiokande (0.5 Mton) data taking. The red and blue histograms are for the  $e$ -like events directly produced by  $\nu_e$  and  $\bar{\nu}_e$  for two different values of 2-3 mixing. Black histograms correspond to the  $e$ -like events from the invisible muon decays computed, respectively, for  $\cos^2\theta_{23} = 0.35$ , and  $\cos^2\theta_{23} = 0.65$  (dashed lines) and  $\cos^2\theta_{23} = 0.50$  (solid line).

$c_{23}^2 < 0.5$ . The number of  $e$ -like events always increases with  $c_{23}^2$ . This can be used for measurements of  $c_{23}^2$ .

Tagging of neutrons allows one to detect the total signal produced by antineutrinos:  $\bar{\nu}_e$  and  $\bar{\nu}_\mu$ . One can further disentangle the contributions from electron and muon antineutrinos by making the fit of spectral shape and using the known spectrum of positrons from the muon decay at rest. This contribution is characterized by a single normalization parameter which can be then extracted from the data fit.

If no neutron tagging occurs, one measures the total energy spectrum of electrons and positrons (see Figs. 8 and 9). As follows from the figures, even in this case one can extract certain information on deviation of the 2-3 mixing from maximal and on the 1-3 mixing.

As we have mentioned before, different components of the spectrum have different dependence on the solar activity. This allows one, in principle, to disentangle the direct  $\nu_e$ - and  $\bar{\nu}_e$  signal and the signal from the invisible muon decays (muon neutrinos).

High statistics of future experiments will open a possibility to play with other characteristics such as angular distributions, directionality, and time dependence. Also, detection of the neutral current events can provide important information.

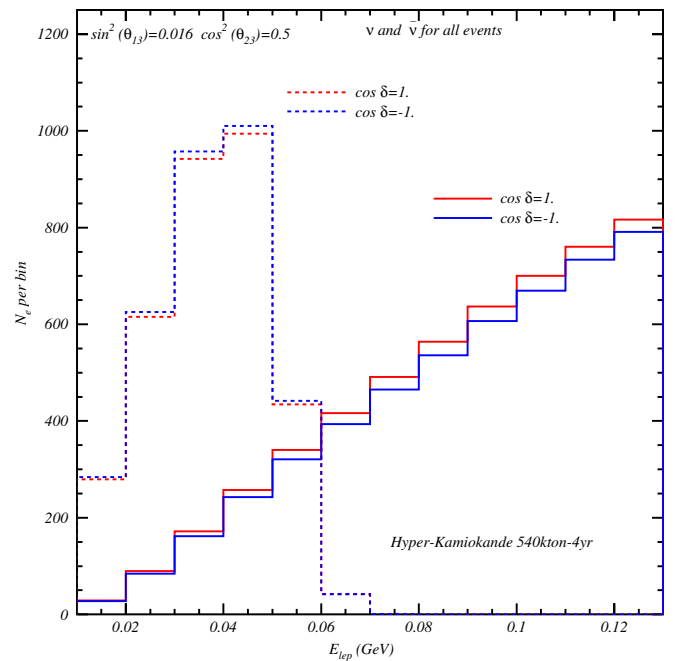


FIG. 9 (color online). Effect of the 1-3 mixing on the spectra of  $e$ -like events. The total number of  $e$ -like events induced by  $\nu_e$ ,  $\bar{\nu}_e$ , and invisible muons decays for the HyperKamiokande 4 years of data taking is given as a function of the charged lepton energy. Shown are the histograms for  $c_{23}^2 = 0.5$ ,  $s_{13}^2 = 0.016$ ,  $\cos\delta = +1$ , and  $\cos\delta = -1$ .

A very detailed study of the sub-sub-GeV events including determination of the flavor and charge of the produced lepton will be possible with large volume liquid Ar detectors [23–25].

## X. CONCLUSION

- (1) There are several new features which appear at low energies ( $E \lesssim 100$  MeV) in the production, oscillations, and detection of the atmospheric neutrinos. One of these features is a substantial decrease of the flavor ratios with a decrease of energy and their substantial deviation from 2 in very low energy bins. As far as oscillations are concerned, there is strong averaging of oscillations due to integration over the angular variables. The oscillations in the atmosphere become important. For events induced by the electron neutrinos, the energy of an electron (positron) is practically related to the energy of a neutrino. In contrast, for muon neutrinos detected via the decays of invisible muons, information on the neutrino energy is practically lost. These events are induced, mainly, by neutrinos in the energy interval (0.1–0.3) GeV.
- (2) We performed both numerical and analytical study of the oscillations of sub-sub-GeV neutrinos. Dependence of the oscillation effects on  $\sin\theta_{13}$ ,  $\delta$  and deviation of the 2-3 mixing from maximal are given explicitly. For the rest, one can use either numerical results or semianalytical formulas.
- (3) For neutrino trajectories below the horizon, one should take into account the oscillations in a two-layer medium: the atmosphere and the Earth. We have presented the relevant oscillation probabilities and numbers of events as functions of  $\sin\theta_{13}$ ,  $\delta$ , and  $\theta_{23}$  and in terms of  $P_2$ ,  $R_2$ , and  $I_2$ . For the latter we give precise semianalytical formulas using the Magnus expansion as well as explicit expressions for the constant density.
- (4) For the  $e$ -like events at  $s_{13} = 0$ , the corrections due to the oscillations driven by the 1-2 mixing can be as large as 10%–15% depending on possible deviations of the 2-3 mixing from maximal. The oscillations lead to a change of the total number of events and also to a distortion of the energy spectrum. The distortion is stronger in the low energy bins. The effect (change of the slope of the spectrum in the interval 10–100 MeV) can be as large as (7–8)%.
- (5) The 1-3 mixing leads to an additional, somehow smaller, effect. For maximal allowed values  $s_{13}^2 \approx 0.03$ , it can reach  $\pm 4\%$  at low energies and  $\pm 6\%$  at high energies. The energy dependence of the effect is stronger for  $\nu_e$ . The linear corrections which dominate at low energies vanish in the resonance  $E \sim 100$  MeV. For antineutrinos, corrections slightly decrease with energy. The corrections for

antineutrinos are much larger than for neutrinos at  $E \sim 100$  MeV.

- (6) In the energy interval (0.1–0.3) GeV, the  $\nu_\mu$  flux is detected via the decay of invisible muons. The total number of  $e$ -like events from these muons depends on the 2-3 mixing in the lowest order. For allowed values of the deviation of the 2-3 mixing from maximal, the effect can be as large as 5%. Inclusion of the 1-2 mixing gives (for  $s_{13} = 0$ ) a maximum 5% effect for neutrinos and 3% effect for antineutrinos. This maximal value is realized at  $c_{23}^2 = 0.65$ . For  $c_{23}^2 < 0.5$  the effect is smaller. The 1-3 mixing produces comparable to 1-2 mixing corrections. The largest effect is for antineutrinos and  $c_{23}^2 = 0.65$ :  $\epsilon_\mu^{(1)} \sim 0.02$ . The linear in  $s_{13}$  correction is strongly suppressed for neutrinos. The quadratic corrections are not negligible and can be of the order of 0.01.
- (7) There is strong degeneracy of parameters  $s_{13} \cos\delta$  and  $c_{23}^2$ , especially for the invisible decays. Inclusion of the 1-3 mixing effects only slightly enlarges the region of possible values of ratio  $N_\mu/N_\mu^0$ .
- (8) The signals from interactions of 4 different fluxes  $\nu_e$ ,  $\nu_\mu$ ,  $\bar{\nu}_e$ , and  $\bar{\nu}_\mu$  can be disentangled by tagging the accompanying neutrons and studying the shape of energy spectrum as well as the time dependence of signals. Confronting events of different types as well as events at low and high energies allows one to reduce the degeneracy of oscillation parameters.
- (9) The number of presently detected events (at SuperKamiokande I) due to the interactions of very low energy neutrinos is about a few hundred which provides an accuracy of determination of the oscillation parameters not better than 10%, and an additional problem is uncertainties of neutrino fluxes. So, to study oscillation effects discussed in this paper, one needs much larger statistics which can be achieved with the megaton-scale detector.
- (10) The low energy atmospheric neutrinos can be used to measure deviation of 2-3 mixing from maximal, the 1-3 mixing, and the phase  $\delta$ . They can be used to search for new physics. Apparently, for the latter, knowledge of the standard oscillation effects computed in this paper is necessary. Understanding of the fluxes of these neutrinos is also important for future studies of the relic supernova neutrinos.

## APPENDIX A: PROBABILITIES $P_2$ , $R_2$ , AND $I_2$ IN THE SECOND ORDER OF THE MAGNUS EXPANSION

The probability functions **D** in the second order Magnus expansion can be found using definitions (24) and results of [15]:

$$\begin{aligned}
P_2 &= \left[ \left( \cos I_{\text{tot}} \sin \phi^{ad} - \frac{I_{\theta\theta}}{I_{\text{tot}}} \sin I_{\text{tot}} \cos \phi^{ad} \right) \sin 2\theta_m^0 + \frac{I_{\theta}}{I_{\text{tot}}} \sin I_{\text{tot}} \cos 2\theta_m^0 \right]^2, \\
R_2 &= -\frac{1}{2} \sin 4\theta_m^0 \left[ \left( \cos I_{\text{tot}} \sin \phi^{ad} - \frac{I_{\theta\theta}}{I_{\text{tot}}} \sin I_{\text{tot}} \cos \phi^{ad} \right)^2 - \left( \frac{I_{\theta}}{I_{\text{tot}}} \right)^2 \sin^2 I_{\text{tot}} \right] \\
&\quad - \cos 4\theta_m^0 \left( \cos I_{\text{tot}} \sin \phi^{ad} - \frac{I_{\theta\theta}}{I_{\text{tot}}} \sin I_{\text{tot}} \cos \phi^{ad} \right) \frac{I_{\theta}}{I_{\text{tot}}} \sin I_{\text{tot}}, \\
I_2 &= \frac{1}{2} \cos^2 I_{\text{tot}} \sin 2\theta_m^0 \sin 2\phi^{ad} + \frac{I_{\theta}}{2I_{\text{tot}}} \sin 2I_{\text{tot}} \cos 2\theta_m^0 \cos \phi^{ad} + I_{\theta\theta} \left[ -\frac{\sin 2I_{\theta}}{2I_{\text{tot}}} \sin 2\theta_m^0 \cos 2\phi^{ad} \right. \\
&\quad \left. - \frac{I_{\theta\theta}}{2I_{\text{tot}}^2} \sin^2 I_{\text{tot}} \sin 2\theta_m^0 \sin 2\phi^{ad} + I_{\theta} \frac{\sin^2 I_{\theta}}{I_{\text{tot}}^2} \cos 2\theta_m^0 \sin \phi^{ad} \right]. \tag{A1}
\end{aligned}$$

Here

$$I_{\text{tot}} \equiv \sqrt{I_{\theta}^2 + I_{\theta\theta}^2},$$

and

$$I_{\theta\theta} = 4 \int_{\bar{x}}^{x_f} dx \int_{\bar{x}}^x dy \left[ \frac{d\theta_m(x)}{dx} \right] \left[ \frac{d\theta_m(y)}{dy} \right] \sin \phi^{ad}(x) \cos \phi^{ad}(y).$$

## APPENDIX B: FUNCTIONS $\tilde{\mathbf{D}}$ FOR TWO LAYERS

According to Eqs. (38), (14), and (37), the elements of the  $S$  matrix in the two-layer case equal

$$\begin{aligned}
\tilde{A}_{ee} &= A'_{ee}(c_{\phi} + i \cos 2\theta_{12} s_{\phi}) - iA'_{e\mu} \sin 2\theta_{12} s_{\phi}, & \tilde{A}_{e\mu} &= A'_{e\mu}(c_{\phi} - i \cos 2\theta_{12} s_{\phi}) - iA'_{ee} \sin 2\theta_{12} s_{\phi}, \\
\tilde{A}_{\mu e} &= A'_{\mu e}(c_{\phi} + i \cos 2\theta_{12} s_{\phi}) - iA'_{\mu\mu} \sin 2\theta_{12} s_{\phi}, & \tilde{A}_{\mu\mu} &= A'_{\mu\mu}(c_{\phi} - i \cos 2\theta_{12} s_{\phi}) - iA'_{\mu e} \sin 2\theta_{12} s_{\phi},
\end{aligned} \tag{B1}$$

and  $\tilde{A}_{33} = \exp[-i2(\phi_3^m + \phi_3)]$ , where  $\phi_3^m$  is given in (15) and  $\phi_3$  is the phase acquired in the atmosphere. We present here the probability functions  $\tilde{\mathbf{D}}$  defined as

$$\tilde{A}_{e\mu}^* \tilde{A}_{ee} \equiv R_{e\mu} + iI_{e\mu}, \quad \tilde{A}_{\mu e}^* \tilde{A}_{ee} \equiv R_{\mu e} + iI_{\mu e} \tag{B2}$$

[see also (45)]. Using expressions for the amplitudes (B1), we obtain

$$\begin{aligned}
\tilde{P} &= P_2 + R_2 \sin 4\theta_{12} \sin^2 \phi + I_2 \sin 2\theta_{12} \sin 2\phi + (1-2P_2) \sin^2 2\theta_{12} \sin^2 \phi, \\
R_{e\mu} &= R_2(1-2\cos^2 2\theta_{12} \sin^2 \phi) - I_2 \cos 2\theta_{12} \sin 2\phi - \left( \frac{1}{2} - P_2 \right) \sin 4\theta_{12} \sin^2 \phi, \\
I_{e\mu} &= I_2(1-2\sin^2 \phi) + R_2 \cos 2\theta_{12} \sin 2\phi + \left( \frac{1}{2} - P_2 \right) \sin 2\theta_{12} \sin 2\phi, \\
R_{\mu e} &= R_2(1-2\sin^2 2\theta_{12} \sin^2 \phi) + \frac{R_2 I_2}{P_2} \sin 2\theta_{12} \sin 2\phi - \left( \frac{1}{2} - \frac{R_2^2}{P_2} \right) \sin 4\theta_{12} \sin^2 \phi, \\
I_{\mu e} &= I_2(1-2\sin^2 2\theta_{12} \sin^2 \phi) + \frac{R_2 I_2}{P_2} \sin 4\theta_{12} \sin^2 \phi + \left( \frac{1}{2} - \frac{R_2^2}{P_2} \right) \sin 2\theta_{12} \sin 2\phi. \tag{B3}
\end{aligned}$$

The limit  $P_2 = R_2 = I_2 = 0$  corresponds to oscillations in the atmosphere only (trajectories above the horizon). In this case the probabilities are given by the last terms in each expression which agree with one-layer results (30).

## APPENDIX C: CONSTANT DENSITY CASE

In the constant density approximation, the evolution matrix in matter is given by

$$S' \approx \begin{pmatrix} c_{\phi}^m + i \cos 2\theta_{12}^m s_{\phi}^m & -i \sin 2\theta_{12}^m s_{\phi}^m \\ -i \sin 2\theta_{12}^m s_{\phi}^m & c_{\phi}^m - i \cos 2\theta_{12}^m s_{\phi}^m \end{pmatrix}, \tag{C1}$$

where  $s_{\phi}^m \equiv \sin \phi^m$ ,  $c_{\phi}^m \equiv \cos \phi^m$ , and  $\phi^m$  is the oscillation phase in matter. The total evolution matrix in two layers (vacuum and matter) is  $S^{\text{tot}} = S' S_A$ . Then in the basis  $\nu'$  the amplitudes for two layers  $A_{\alpha\beta} = [S^{\text{tot}}]_{\alpha\beta}$  equal



$$\begin{aligned}
 \tilde{A}_{ee} &= c_\phi^m c_\phi - \cos 2(\theta_{12}^m - \theta_{12}) s_\phi^m s_\phi + i(\cos 2\theta_{12} s_\phi c_\phi^m \\
 &\quad + \cos 2\theta_{12}^m s_\phi^m c_\phi), \\
 \tilde{A}_{e\mu} &= \sin 2(\theta_{12} - \theta_{12}^m) s_\phi^m s_\phi - i(\sin 2\theta_{12} s_\phi c_\phi^m \\
 &\quad + \sin 2\theta_{12}^m s_\phi^m c_\phi), \\
 \tilde{A}_{\mu\mu} &= \tilde{A}_{ee}^*, \quad \tilde{A}_{\mu e} = -\tilde{A}_{e\mu}^*.
 \end{aligned} \tag{C2}$$

The functions  $\tilde{\mathbf{D}}$  (B2) can be presented in the following form:

$$\begin{aligned}
 \tilde{P}^c &= \sin^2 2\theta_{12}^m \sin^2 \phi^m \cos^2 \phi + \sin^2 2\theta_{12} \sin^2 \phi \cos^2 \phi^m \\
 &\quad + \frac{1}{2} \sin 2\theta_{12}^m \sin 2\theta_{12} \sin 2\phi^m \sin 2\phi \\
 &\quad + \sin^2 2(\theta_{12}^m - \theta_{12}) \sin^2 \phi^m \sin^2 \phi,
 \end{aligned} \tag{C3}$$

$$\begin{aligned}
 2R_{e\mu}^c &= -\sin 4\theta_{12}^m \sin^2 \phi^m \cos^2 \phi - \sin 4\theta_{12} \sin^2 \phi \cos^2 \phi^m \\
 &\quad - \sin 2\theta_{12}^m \cos 2\theta_{12} \sin 2\phi^m \sin 2\phi \\
 &\quad + \sin 4(\theta_{12}^m - \theta_{12}) \sin^2 \phi^m \sin^2 \phi,
 \end{aligned} \tag{C4}$$

$$\begin{aligned}
 2I_{e\mu}^c &= \sin 2\theta_{12}^m \sin 2\phi^m \cos^2 \phi + \sin 2\theta_{12} \sin 2\phi \cos^2 \phi^m \\
 &\quad - \sin(4\theta_{12}^m - 2\theta_{12}) \sin 2\phi \sin^2 \phi^m \\
 &\quad - \sin 2\theta_{12}^m \sin^2 \phi \sin 2\phi^m,
 \end{aligned} \tag{C5}$$

$$\begin{aligned}
 2R_{\mu e}^c &= -\sin 4\theta_{12}^m \sin^2 \phi^m \cos^2 \phi - \sin 4\theta_{12} \sin^2 \phi \cos^2 \phi^m \\
 &\quad - \sin 2\theta_{12} \cos 2\theta_{12}^m \sin 2\phi^m \sin 2\phi \\
 &\quad - \sin 4(\theta_{12}^m - \theta_{12}) \sin^2 \phi^m \sin^2 \phi,
 \end{aligned} \tag{C6}$$

$$\begin{aligned}
 2I_{\mu e}^c &= \sin 2\theta_{12}^m \sin 2\phi^m \cos^2 \phi + \sin 2\theta_{12} \sin 2\phi \cos^2 \phi^m \\
 &\quad - \sin(4\theta_{12} - 2\theta_{12}^m) \sin^2 \phi \sin 2\phi^m \\
 &\quad - \sin 2\theta_{12} \sin 2\phi \sin^2 \phi^m.
 \end{aligned} \tag{C7}$$

Notice that in the limit  $\phi \rightarrow 0$  the first term in each expression corresponds to the probability of oscillations in matter, and the second term gives the probability in vacuum ( $\phi_m \rightarrow 0$ ). These two terms are related by the interchange of the vacuum and matter characteristics:  $\theta_m \leftrightarrow \theta$  and  $\phi_m \leftrightarrow \phi$ . The rest is the interference of the oscillation effects in the two layers. The first two terms are the same in  $R_{\mu e}$  and  $R_{e\mu}$  as well as in  $I_{\mu e}$  and  $I_{e\mu}$ ; in turn, these probabilities differ by the interference terms. The probability  $\tilde{P}$  is symmetric with respect to interchange of the matter and vacuum characteristics.

For our discussion it is convenient to write the probabilities in the form given in Eq. (51):

$$\begin{aligned}
 \tilde{P}^c &= \sin^2 2\theta_{12}^m \sin^2(\phi^m + \phi) - (\sin^2 2\theta_{12}^m - \sin^2 2\theta_{12}) \sin^2 \phi \cos^2 \phi^m - \frac{1}{2} \sin 2\theta_{12}^m (\sin 2\theta_{12}^m - \sin 2\theta_{12}) \sin 2\phi \sin 2\phi^m \\
 &\quad + \sin^2(\theta_{12}^m - \theta_{12}) \sin^2 \phi \sin^2 \phi^m, \\
 R_{e\mu}^c &= -\frac{1}{2} \sin 4\theta_{12}^m \sin^2(\phi^m + \phi) - \frac{1}{2} \sin 2\theta_{12}^m (\cos 2\theta_{12} - \cos 2\theta_{12}^m) \sin 2\phi \sin 2\phi^m + \frac{1}{2} \sin^2 \phi [(\sin 4\theta_{12}^m - \sin 4\theta_{12}) \cos^2 \phi^m \\
 &\quad + \sin 4(\theta_{12}^m - \theta_{12}) \sin^2 \phi^m], \\
 R_{\mu e}^c &= -\frac{1}{2} \sin 4\theta_{12}^m \sin^2(\phi^m + \phi) - \frac{1}{2} \cos 2\theta_{12}^m (\sin 2\theta_{12} - \sin 2\theta_{12}^m) \sin 2\phi \sin 2\phi^m + \frac{1}{2} \sin^2 \phi [(\sin 4\theta_{12}^m - \sin 4\theta_{12}) \cos^2 \phi^m \\
 &\quad - \sin 4(\theta_{12}^m - \theta_{12}) \sin^2 \phi^m], \\
 I_{e\mu}^c &= \frac{1}{2} \sin 2\theta_{12}^m \sin 2(\phi^m + \phi) + \frac{1}{2} \sin 2\phi [(\sin 2\theta_{12} - \sin 2\theta_{12}^m) \cos^2 \phi^m + (\sin 2\theta_{12}^m - \sin(4\theta_{12}^m - 2\theta_{12})) \sin^2 \phi^m], \\
 I_{\mu e}^c &= \frac{1}{2} \sin 2\theta_{12}^m \sin 2(\phi^m + \phi) + \frac{1}{2} (\sin 2\theta_{12} - \sin 2\theta_{12}^m) \sin 2\phi \cos^2 \phi^m + \frac{1}{2} [\sin 2\theta_{12}^m - \sin(4\theta_{12} - 2\theta_{12}^m)] \sin^2 \phi \sin 2\phi^m.
 \end{aligned} \tag{C8}$$

## ACKNOWLEDGMENTS

The authors are grateful to G. Battistoni and T. Stanev for discussions of the atmospheric neutrino fluxes at low energies. O. L. G. P. thanks FAPESP, CNPQ, and ICTP for support.

- 
- |   |   |
|---|---|
| <p>[1] G. T. Zatsepin and V. A. Kuzmin, Zh. Eksp. Teor. Fiz. <b>41</b>, 1818 (1961) [Sov. Phys. JETP <b>14</b>, 1294 (1962).]</p> <p>[2] T. K. Gaisser, T. Stanev, S. A. Bludman, and H. S. Lee, Phys. Rev. Lett. <b>51</b>, 223 (1983).</p> <p>[3] T. K. Gaisser, T. Stanev, and G. Barr, Phys. Rev. D <b>38</b>, 85 (1988).</p> | <p>[4] M. Honda, T. Kajita, K. Kasahara, and S. Midorikawa, Phys. Rev. D <b>52</b>, 4985 (1995).</p> <p>[5] M. Honda, K. Kasahara, and S. Midorikawa, Phys. Lett. B <b>248</b>, 193 (1990).</p> <p>[6] G. Battistoni, A. Ferrari, T. Montaruli, and P. R. Sala, Astropart. Phys. <b>23</b>, 526 (2005).</p> |
|---|---|

- [7] M. Malek *et al.* (SuperKamiokande Collaboration), Phys. Rev. Lett. **90**, 061101 (2003).
- [8] M.S. Malek, Report No. UMI-31-06530, available at <http://wwwsk.icrr.u-tokyo.ac.jp/sk/pub/index.html>.
- [9] T. Iida, in *Proceedings of the 30th International Cosmic Ray Conference (ICRC), Merida, Yucatan, Mexico*, available at <http://indico.nucleares.unam.mx/confSpeakerIndex.py?confId=4>, 2007.
- [10] V.L. Dadykin *et al.*, in *Proceedings of the 12th International Conference Neutrino Physics and Astrophysics Neutrino 1986, 3-8 June 1986, Sendai, Japan*, edited by T. Kitagaki and H. Yuta (World Scientific, Singapore, 1986).
- [11] E.K. Akhmedov, Nucl. Phys. **B538**, 25 (1999); M.V. Chizhov and S.T. Petcov, Phys. Rev. Lett. **83**, 1096 (1999); Phys. Rev. D **63**, 073003 (2001); E.K. Akhmedov, Phys. Lett. B **503**, 133 (2001).
- [12] G.L. Fogli, E. Lisi, A. Mirizzi, and D. Montanino, Phys. Rev. D **70**, 013001 (2004).
- [13] G.L. Fogli, E. Lisi, A. Mirizzi, and D. Montanino, J. Cosmol. Astropart. Phys. 04 (2005) 002; A. Mirizzi, in *Proceedings of NOW2004 conference, Conca Specchiulla, Otranto, Lecce, Italy* (unpublished).
- [14] O.L.G. Peres and A.Y. Smirnov, Nucl. Phys. **B680**, 479 (2004).
- [15] A.N. Ioannisian and A.Y. Smirnov, arXiv:0803.1967.
- [16] P. Lipari, M. Lusignoli, and F. Sartogo, Phys. Rev. Lett. **74**, 4384 (1995).
- [17] M.C. Gonzalez-Garcia, H. Nunokawa, O.L.G. Peres, T. Stanev, J.W.F. Valle, Phys. Rev. D **58**, 033004 (1998).
- [18] C.K. Jung, AIP Conf. Proc. **533**, 29 (2000).
- [19] K. Nakamura, Int. J. Mod. Phys. A **18**, 4053 (2003).
- [20] L. Mosca, Nucl. Phys. B, Proc. Suppl. **138**, 203 (2005).
- [21] D. Autiero *et al.*, J. Cosmol. Astropart. Phys. 11 (2007) 011.
- [22] J.F. Beacom and M.R. Vagins, Phys. Rev. Lett. **93**, 171101 (2004).
- [23] A.G. Cocco, A. Ereditato, G. Fiorillo, G. Mangano, and V. Pettorino, J. Cosmol. Astropart. Phys. 12 (2004) 002.
- [24] D.B. Cline, F. Raffaelli, and F. Serigiampietri, JINST **1**, T09001 (2006).
- [25] A. Ereditato and A. Rubbia, Nucl. Phys. B, Proc. Suppl. **155**, 233 (2006).